Quaternary Science Reviews 313 (2023) 108198

Contents lists available at ScienceDirect

Quaternary Science Reviews

journal homepage: www.elsevier.com/locate/quascirev

Invited paper

Sea ice variability in the North Atlantic subpolar gyre throughout the Last Interglacial

Kristine Steinsland [a, *], Danielle M. Grant [a], Ulysses S. Ninnemann [b], Kirsten Fahl [c], Ruediger Stein [c, d, e], Stijn De Schepper [a]

[a] NORCE Climate and Environment, NORCE Norwegian Research Centre AS and Bjerknes Centre for Climate Research, Bergen, Norway
[b] University of Bergen, Department of Earth Science and Bjerknes Centre for Climate Research, Bergen, Norway
[c] Alfred Wegener Institute Helmholtz Centre for Polar and Marine Research, Bremerhaven, Germany
[d] University of Bremen, Faculty of Geosciences and Center for Marine Environmental Sciences, Bremen, Germany
[e] Ocean University of China, Frontiers Science Center for Deep Ocean Multispheres and Earth System and Key Laboratory of Marine Chemistry Theory and Technology, Qingdao, China

ARTICLE INFO

Article history:
Received 11 November 2022
Received in revised form
20 June 2023
Accepted 20 June 2023
Available online 9 July 2023

Handling Editor: A. Voelker

Keywords:
Sea ice
Labrador sea
Eirik drift
Ocean circulation
Dinoflagellate cysts
Biomarkers
IP_{25}
MIS 5e

ABSTRACT

The Last Interglacial period, Marine Isotope Stage 5e (MIS 5e ~116–128 ka), is thought to have had a warmer, but less stable climate than the present interglacial. One key factor that has the potential to influence the ocean and climate is sea ice, but its presence and extent throughout MIS 5e is poorly constrained. Here we reconstruct the sea surface hydrography and sea ice variability in the Labrador Sea, a region influenced by the subpolar gyre (SPG) and where deep water formation occurs, in order to evaluate the potential of sea ice to drive or amplify ocean variability. We analysed biomarkers (highly branched isoprenoids, HBIs, and sterols), dinoflagellate cyst assemblages and stable oxygen isotopes from the late stages of MIS 6, throughout MIS 5e, into MIS 5d. Our results show that the late glacial MIS 6 was likely characterised by a thick multiyear sea ice cover. During the first phase of MIS 5e, the hydrography was highly variable. The initial 1500 years (128–126.5 ka) were characterised by the presence of a seasonal Marginal Ice Zone (MIZ) accompanied by subsurface warmth. As the sea ice retreated, cool, likely polar-sourced water dominated the surface and subsurface ocean (126.5–124 ka), until an abrupt surge of sea ice marked the final pulse of the remnants of the deglaciation. The second half of MIS 5e (124–116 ka) was characterised by a persistent inflow of warm water, only interrupted by incursions of cold water as summer insolation declined. Seasonal sea ice returned to the Eirik Drift during MIS 5d. We infer that sea ice variability throughout MIS 5e was coupled with the variability of the SPG. Especially the location of a proximal MIZ to the Labrador Sea convection region could have been important for SPG dynamics. In addition, the presence of sea ice at the transitions into and out of MIS 5e could point to its important role in modulating and enhancing the magnitude and coherence of climate signals at major climatic transitions.

1. Introduction

The potential climatic implications of global warming can be understood by investigating past periods in Earth's history which were as warm or warmer than today. Although there is no perfect analogue, the Last Interglacial (LIG; 116–128 ka), Marine Isotope Stage 5e (MIS 5e), has many features in common with model projections of future climate. These features include a warmer than present global climate, a significantly reduced Greenland Ice Sheet (GIS), and a higher sea level (e.g. Otto-Bliesner et al., 2006; Kopp et al., 2009). For this reason, the LIG has sparked the interest of many studies, aiming to understand climate variability, instability, and their underlying mechanisms.

Sea ice has been proposed as a cause for variability and instability of the North Atlantic Ocean circulation during the LIG due to its potential effect on the subpolar gyre (SPG; Born et al., 2010; Galaasen et al., 2014; Li and Born, 2019; Kessler et al., 2020). Sea ice can change rapidly in response to relatively weak forcing and it can amplify climate change non-linearly, resulting in rapid and large

* Corresponding author.
E-mail address: stei@norceresearch.no (K. Steinsland).

https://doi.org/10.1016/j.quascirev.2023.108198
0277-3791/

climate shifts. The SPG has been suggested to be integrally connected to the larger scale circulation and the Atlantic Meridional Overturning Circulation (AMOC; e.g. Hátún et al., 2005; Thornalley et al., 2009; Yeager, 2015; Klockmann et al., 2020), and thus it serves as one link in the chain of global teleconnections that alters climate on a global scale. The SPG is sensitive to buoyancy and wind forcing (e.g. Born and Stocker, 2014; Levermann and Born, 2007; Montoya et al., 2011) whereas the extent of sea ice influences both these forcings. Furthermore, buoyancy forcing affects deep water formation in the North Atlantic, which in turn affects the strength of the AMOC. Thus, in the Labrador Sea where deep water formation occurs, the SPG could be especially sensitive to the extent of sea ice and its associated freshwater (Born et al., 2010; Li and Born, 2019). It has been suggested that a strong SPG may also tend to expand zonally (eastward), redirect Atlantic waters into the westward flowing Irminger Current (IC) and corresponds to a weak AMOC (Klockmann et al., 2020). In contrast, a weak SPG contracts to the west, directs Atlantic waters northeast into the Nordic Seas, contributing to persistent deep water formation there (Thornalley et al., 2009) and corresponds to a strong AMOC (Hátún et al., 2005; Häkkinen and Rhines, 2004). However, it does remain unclear exactly how tightly coupled gyre size and strength are (Foukal and Lozier, 2017), and how or if they contributed to recent changes in overturning circulation (Lozier, 2012; Lozier et al., 2019). Thus, based on the brief observational period, it is difficult to draw conclusions about how SPG geometry, strength, and the basin scale overturning circulation are linked. Despite the complex circulation coupling, the SPG's potential to alter mass, heat, and buoyancy, and alter climate across the North Atlantic, and beyond, makes it crucial to understand the mechanisms by, and timescales on, which the SPG can vary. In this study, we focus on the potential of sea ice and its associated feedbacks on SPG and North Atlantic Ocean variability during the LIG.

Fossil assemblages and biomarkers preserved in marine sediments are frequently used for sea ice reconstructions (e.g. de Vernal et al., 2013). While several proxies are indirectly related to sea ice, the biomarker IP_{25} is exclusively biosynthesized by a few diatom species living in Arctic sea ice (Brown et al., 2014; Limoges et al., 2018) and provides a sensitive and reliable sea ice indicator. LIG sea ice reconstructions based on biomarkers are restricted to the Arctic Ocean (Stein et al., 2017, 2022; Kremer et al., 2018a, 2018b). No biomarker records exist from the LIG subpolar North Atlantic. Specifically for the Labrador Sea, biomarker-based sea ice reconstructions are only available for part of MIS 3 (Scoto et al., 2022) and the last Glacial to Holocene (You et al., 2023). For the LIG time interval from this area, on the other hand, sea ice reconstructions are mainly based on dinoflagellate cyst (*hereafter* dinocyst) transfer functions and assemblages (e.g. Eynaud et al., 2004; Hillaire-Marcel et al., 2001; de Vernal and Hillaire-Marcel, 2008; Penaud et al., 2008; Van Nieuwenhove et al., 2011), and indirect inferences based on foraminifer assemblages (e.g. Irvali et al., 2012, 2016). A compilation of sea ice records by Kageyama et al. (2021) demonstrates that north of 79°N the LIG sea ice concentrations range from minimal to substantial (>75%) all year around. South of 79°N, the Atlantic and Nordic Seas were sea ice free during the LIG. This partly contrasts previous studies suggesting that sea ice and its associated melt in the Labrador Sea could modulate SPG circulation on centennial timescales within the LIG (Galaasen et al., 2014), and during the last glacial inception (Born et al., 2010). These authors speculate and/or infer sea ice presence from indirect proxies and modelling experiments but biomarker data that can unequivocally document sea ice presence is lacking. This highlights our limited knowledge about sea ice extent and variability in the North Atlantic SPG region, which is crucial in order to evaluate its role in modulating ocean circulation and the SPG on glacial-interglacial timescales.

Here we reconstruct sea ice occurrence, marginal ice zone (MIZ; transition between open ocean and sea ice) extent, and surface ocean hydrography from the late glacial stage of MIS 6 throughout MIS 5e, and into MIS 5d using dinocyst assemblages, biomarkers (IP_{25}) and stable oxygen isotopes from an Eirik Drift sediment core. We combine our data with previously published foraminifer records from the same region, and with other North Atlantic records to gain a broader understanding of the Labrador Sea surface hydrography, the surface currents of the SPG and the larger scale North Atlantic surface ocean variability.

2. Site location and oceanography

The Eirik Drift is a sediment drift located off the southern tip of the Greenland margin and is well situated to monitor changes in the northwest SPG that dominates the hydrography of the North Atlantic (Hátún et al., 2005). It is characterised by high sedimentation rates sustained by eroded sediments imported primarily by Denmark Strait Overflow Water and deposited here along the most offshore portion of the Deep Western Boundary Current (DWBC) (Wold, 1994; Hunter et al., 2007), leading to expanded sedimentary interglacial intervals (Hillaire-Marcel et al., 1994). The surface ocean hydrography at the Eirik Drift is characterised by the cyclonic circulation of the SPG, which is fed by the North Atlantic Current (NAC) from the south, and the East Greenland Current (EGC) from the north (Fig. 1). The NAC transports warm and salty Atlantic waters northward as an extension of the Gulf Stream, branching into the Norwegian Atlantic Current (NwAC) flowing northward, and the IC flowing west and forming the east part of the SPG circulation pattern. The EGC flows southward from the Arctic Ocean, via the Denmark Strait, into the North Atlantic and is a major contributor of cold, fresh surface water to the vicinity of the study area (Bacon et al., 2002).

3. Material and methods

In 2016, calypso Core GS16-204-22CC-B (*hereafter* 22CC-B; 58°02.83′N, 47°02.36′W; 3160 m water depth) was collected from the Eirik Drift with the research vessel G.O. Sars. Based on lithological description of this core, and a preliminary correlation (oxygen isotopes, colour scan) to the well-dated Core MD03-2664 (57°26.34′N, 48°36.35′W; 3440 m water depth; Irvali et al., 2012, 2016), we first estimated MIS 5e to occur between 14.5 and 18.5 m core depth. The samples for this study were collected at different times and for different purposes. During the initial sampling, we collected 1.5 cm thick sediment samples at 4 cm resolution for sedimentary ancient DNA (*seda*DNA), palynology, foraminifers and biomarkers for the entire study interval (1456–1852 cm). In the second sampling phase, we sampled in-between the first sample set at higher resolution and with thinner sediment samples (0.7–0.8 cm) for part of the core (1556–1753.5 cm).

Dinocyst assemblages were analysed every 4 cm, except in MIS 6 (1756–1852 cm) where we analysed every 12 cm. Biomarkers and foraminifers were prioritised for a higher resolution sampling at obvious transitions in the core. Biomarkers were analysed at every ~2 cm between 1555 and 1648 cm, and at every ~1 cm between 1648 and 1756 cm. Foraminifers were analysed at the same resolution as the biomarkers (every ~1 cm) between 1704 and 1756 cm. For the rest of the core, sampling was done every 4 cm. For exact sampling depths, and intervals, see Supplementary Data.

3.1. Stable isotopes

Stable oxygen isotope analyses ($\delta^{18}O$) were performed on the planktic foraminifer *Neogloboquadrina pachyderma* (sinistral) and

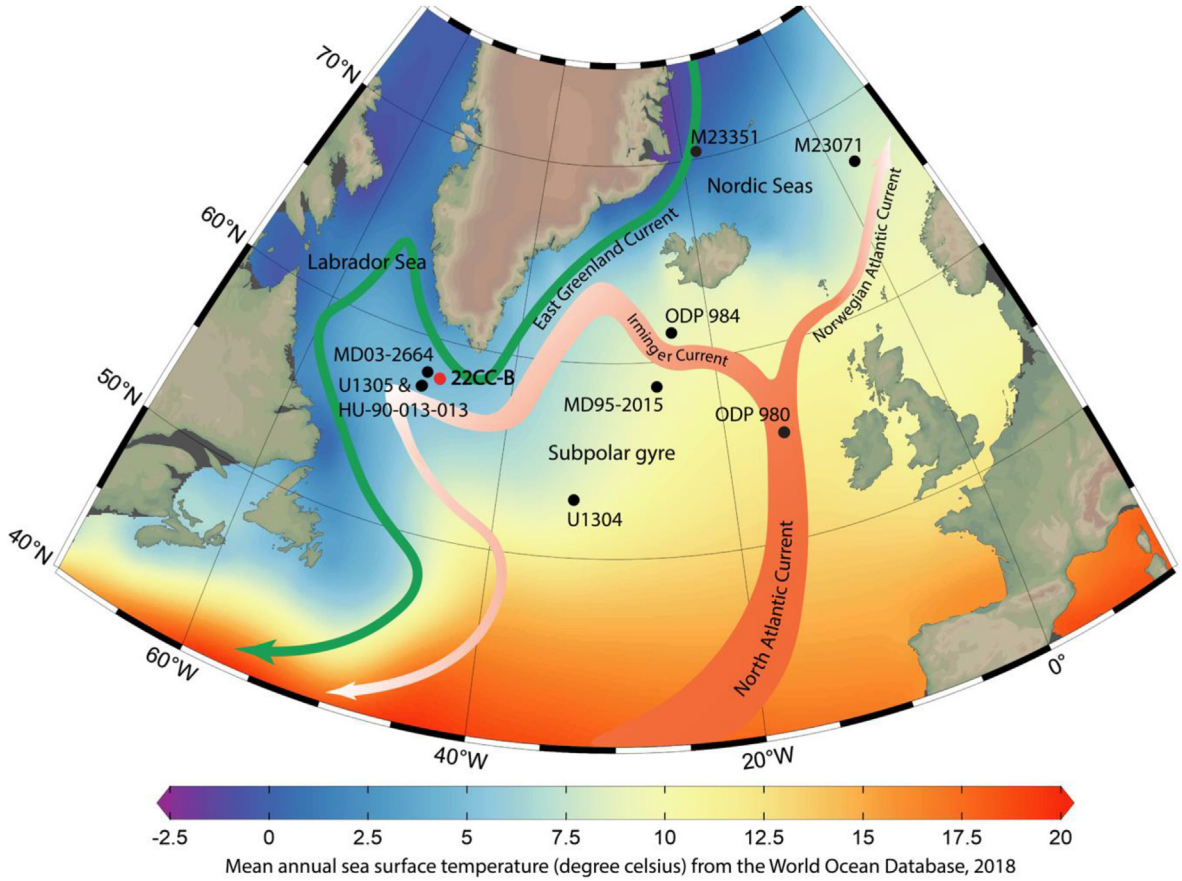

Fig. 1. Mean annual sea surface temperatures from WOA 2018 (Locarnini et al., 2019) and major surface ocean currents relative to our studied Core GS16-204-22CC-B (red dot). Other sediment records (black dots) discussed in the text are from MD03-2664 (Irvali et al., 2012, 2016; Galaasen et al., 2014), IODP Sites U1304 and U1305 (Channell et al., 2006), ODP Sites 984 (Mokeddem et al., 2014) and 980 (Oppo et al., 2006), HU-90-013-013 (Hillaire-Marcel et al., 1994), MD95-2015 (Eynaud et al., 2004), M23071 (Van Nieuwenhove et al., 2008), and M23351 (Zhuravleva et al., 2017).

benthic foraminifer *Cibicidoides wuellerstorfi* in order to constrain the chronology of MIS 5e. *N. pachyderma* (s) was identified in all samples, while *C. wuellerstorfi* was absent in ~1/3 of the samples (see Supplementary Data). A Finnigan MAT253 mass spectrometer with an online Kiel IV, located at FARLAB, University of Bergen, was used for the stable isotope analysis. Values are reported relative to Vienna Pee Dee Belemnite. Two working standards (CM12 and Riedel) along with 2 international standards (NBS-18 and NBS-19) were analysed each day interspersed with samples. The external precision for samples between 10 and 100 μg was better than 0.08 and 0.04‰ for $\delta^{18}O$ and $\delta^{13}C$, respectively, based on the long-term reproducibility (1σ) of the working standard CM12.

3.2. Total organic carbon, biomarkers and their ecological significance

A total of 187 samples were analysed for biomarkers (HBIs and sterols) and 254 samples for Total Organic Carbon (TOC)%. Biomarkers and TOC were measured and analysed at the Alfred Wegener Institute in Bremerhaven, Germany. To determine the TOC (%), 100 μg of freeze-dried and homogenised sediments were measured (per sample) using an ELTRA CS2000 Carbon Sulfur Detector. For biomarker analysis preparation, 5 g of freeze-dried sediments was homogenised using an agate mortar. Prior to extraction, the internal standards 7-hexylnonadecane (7-HND: 0.0038 μm/ml), androstanol (0.05 μm/ml), 9-octylheptadec (9-OHD: 0.005 μm/ml), and squalane (0.032 μm/ml) were added to the sediments to allow for later stage quantification. Biomarkers were extracted by sonication (3 × 15 min) using dichloromethane:methanol (2:1 v/v; 30 ml) as solvent. The extract was separated into hydrocarbon and sterol fractions through open-column chromatography (5 ml *n*-hexane for hydrocarbons and 9 ml ethylacetate:*n*-hexane (4:1) for sterols) with silica gel (SiO_2) as the stationary phase. The sterol fraction was silyated with 200 μl BSTFA (bis-trimethylsilyl-trifluoracet-amide; 60 °C for 2 h). Biomarker analysis was performed by gas chromatography-mass-spectrometry (GC-MS). Hydrocarbon concentrations were determined with a gas chromatograph Agilent Technologies 7890 GC (30 m HP-1MS column, 0.25 mm in diameter and 0.25 μm film thickness) coupled to an Agilent Technologies 5977 A mass selective detector. Sterol concentrations were measured with a gas chromatograph Agilent Technologies 6850 GC (30 m HP-1MS column, 0.25 mm in diameter and 0.25 μm film thickness) coupled to an Agilent Technologies 5975 A mass selective detector. HBIs (IP_{25}, HBI II, HBI III (Z), HBI III (E)) and sterols were identified by comparing their retention times to those of reference compounds (IP_{25}: Belt et al., 2007; HBI II: Johns et al., 1999; HBI III: Belt et al., 2000; sterols: Boon et al., 1979; Volkman, 1986). IP_{25}, HBI II, HBI III (Z), and HBI III (E) (IP_{25}: m/z 350; HBI II: m/z 348; HBI III (Z) and (E): m/z 346) were quantified by the abundant fragment ion m/z 266 of the internal standard 7-HND. Sterols were quantified as trimethylsilyl ethers (brassicasterol: m/z 470, campesterol: m/z 472, sitosterol: m/z 486, dinosterol: m/z 500) in regard to the molecular ion of androstanol (ion m/z 348). The different responses

of all these ions were balanced by external calibration. Instrument stability was controlled by reruns of external standards and replicate analyses for random samples. All biomarker concentrations have been normalised to the TOC.

The sea ice proxy IP_{25} (Ice Proxy with 25 carbon atoms) is a molecule produced by a relatively small number of diatoms that inhabit the base of Arctic sea ice (Brown et al., 2014; Limoges et al., 2018) and is predominantly found in areas covered by seasonal sea ice (Belt et al., 2007; Xiao et al., 2015; Kolling et al., 2020; for review see Belt, 2018). In this study, we consider the occurrence of IP_{25} as a sea ice indicator. A difficulty with IP_{25} is that both permanent sea ice environments and open water conditions are characterised by IP_{25} concentrations of zero. Under permanent sea ice conditions, IP_{25} is absent due to limited light and nutrient availability which are required for the growth of sea ice phytoplankton. Likewise, in open waters, the habitat for the ice algae is missing, and IP_{25} concentrations are zero. The ambiguity of the signal from permanent sea ice *vs* open ocean requires that IP_{25} is analysed in combination with open-water phytoplankton biomarkers like brassicasterol and dinosterol (cf. Müller et al., 2009, 2011). These are produced by a variety of phytoplankton genera like dinoflagellates, diatoms and haptophytes (Boon et al., 1979; Robinson et al., 1984; Volkman et al., 1998). Alongside IP_{25}, several other biomarkers are related to sea ice. HBI III (Z) is a common constituent of marine settings (Belt et al., 2000) but shows a more direct association with MIZ productivity (Collins et al., 2013; Belt et al., 2015). HBI II is produced by sea ice/land-fast ice-dwelling diatoms in the Southern Ocean (Belt et al., 2016). Although its origin and potential as an environmental proxy in the Northern Hemisphere is unclear, it is often observed together with IP_{25}. Thus, Belt et al. (2018) postulate that HBI II might represent an "even better" sea ice proxy than IP_{25} or at least be a useful substitute in cases where IP_{25} is absent. Terrigenous influence can be inferred by sitosterol and campesterol (Pryce, 1971; Huang and Meinschein, 1979). Although these biomarkers are found in a few microalgae species, the main contributors are higher land plants (Volkman, 1986; Jaffé et al., 1995; Rontani et al., 2014).

3.3. Dinoflagellate cyst assemblages and ecological significance

A total of 85 samples were selected for dinocyst assemblage analysis and prepared using a standard palynological preparation procedure (e.g. De Schepper et al., 2017). To remove the mineral fraction, cold hydrochloric and hydrofluoric acid was used. The palynological residue was sieved over a 10 μm polymer mesh before mounting on slides with glycerine jelly. One tablet of *Lycopodium clavatum* spores (batch #140119321, n = 19,855 ± 521 spores per tablet) was added to each sample before chemical treatment to allow calculation of dinocyst concentrations and errors following Stockmarr (1971). The palynological slides were counted at 400× magnification for dinocyst assemblage analyses until a minimum of 300 *in situ* dinocysts were identified. If the dinocyst concentration was too low to reach the minimum threshold, the entire slide (ca. 20 non-overlapping traverses) was counted. We identified 38 dinocyst taxa in total. The major dinocyst taxa consist of *Bitectatodinium tepikiense*, *Operculodinium centrocarpum* sensu Wall and Dale (1966) (hereafter *O. centrocarpum*), *Nematosphaeropsis labyrinthus* and the group of Round Brown cysts (RBC). *Brigantedinium* specimens were grouped together as RBC because folding or orientation of specimens often limited identification to species level. *Spiniferites* spp. includes all *Spiniferites* cysts except *S. elongatus* and *S. mirabilis*. All *Impagidinium* species identified were grouped together with the exception of *I. pallidum*. These grouped species include *I. aculeatum, I. sphaericum, I. paradoxum, I. patulum* and *I. plicatum*.

The distribution of dinoflagellates depends on physical and chemical sea surface parameters such as currents, temperature, salinity, irradiance, nutrients and sea ice (e.g. de Vernal et al., 2020). Their different environmental preferences make them suited for surface ocean reconstructions.

B. tepikiense is linked to the subpolar-temperate transition in the North-Atlatic (Dale, 1996) and also enhanced water stratification (Rochon et al., 1999; de Vernal et al., 2005; de Vernal and Marret, 2007; Hennissen et al., 2014). The species has a high tolerance to a wide range of salinities and temperatures and it can be observed in regions that are seasonally covered by sea ice for less than 4 months a year (de Vernal et al., 1997). In modern sediments from the Labrador Sea and North Atlantic, *B. tepikiense* rarely exceeds >10% of the assemblage (e.g. de Vernal et al., 2005, 2020). During the Last Glacial Maximum, *B. tepikiense* makes up more than 50% of the assemblage in the northern North Atlantic (de Vernal et al., 2005). Thus, the species is characteristic for conditions different than present and is not common in warm interglacial periods. *N. labyrinthus* is another subpolar-temperate species (Rochon et al., 1999; Marret and Zonneveld, 2003) that has been linked to climate transitions (i.e. glacial–interglacial) when profound changes in water mass composition occurred (Hennissen et al., 2017, and references therein).

The distribution of *O. centrocarpum* in modern surface sediments of the North Atlantic reveals that high relative abundances are linked to warm Atlantic Water (e.g. NAC/NwAC), although it is generally a cosmopolitan taxon (e.g. Marret and Zonneveld, 2003). In fossil records from the Arctic and sub-Arctic, *O. centrocarpum* is often regarded as an indicator for interglacial intervals with Atlantic water advection (e.g. Rochon et al., 1999; Matthiessen et al., 2001; Matthiessen and Knies, 2001; Grøsfjeld et al., 2006). Also *S. mirabilis* is an indicator of warm temperate to temperate environments. Previous studies have linked this species to interglacial optima in the northern North Atlantic during MIS 5 (Sánchez Goñi et al., 1999; Eynaud et al., 2004; Penaud et al., 2008; Van Nieuwenhove et al., 2008, 2011).

Other environmentally significant species in our record include the RBC and the cysts of *Pentapharsodinium dalei* indicating sea ice and surface ocean stratification respectively. The RBC are a group of heterotrophic taxa that strongly relate to the trophic state of the surface waters in addition to temperature and salinity (e.g. de Vernal et al., 2000). In environments with increased nutrient availability like frontal zones and sea ice margins, RBC and heterotrophic dinocyst taxa commonly outnumber other dinocysts (e.g. de Vernal et al., 2020). In our record, the cysts of *P. dalei* are found in combination with the RBC. In the Arctic and sub-Arctic oceans high proportions of cysts of *P. dalei* are found in stratified and productive waters at a distance from the multiyear sea-ice zone (Radi et al., 2001; Marret et al., 2004; Solignac et al., 2009) and in fjords receiving a spring freshet of glacier meltwater (Dale, 2001; Grøsfjeld et al., 2009).

4. Results

4.1. Chronology

The age model for Site 22CC-B (Fig. 2) is based on aligning our benthic (*C. wuellerstorfi*) $\delta^{18}O$ record with the benthic $\delta^{18}O$ isotopic record from the nearby Core MD03-2664 (Irvali et al., 2012, 2016), using AnalySeries (Paillard et al., 1996). Previous studies (Irvali et al., 2012, 2016; Galaasen et al., 2014) tuned Core MD03-2664 to MD95-2042 on the Iberian Margin (Shackleton et al., 2002, 2003) where the MIS 5e boundaries are set by the benthic isotopic low plateau to 116.1 ± 0.9 ka and 128 ± 1 ka based on fossil coral reef U-series dates of the LIG sea level high stand (Stirling et al.,

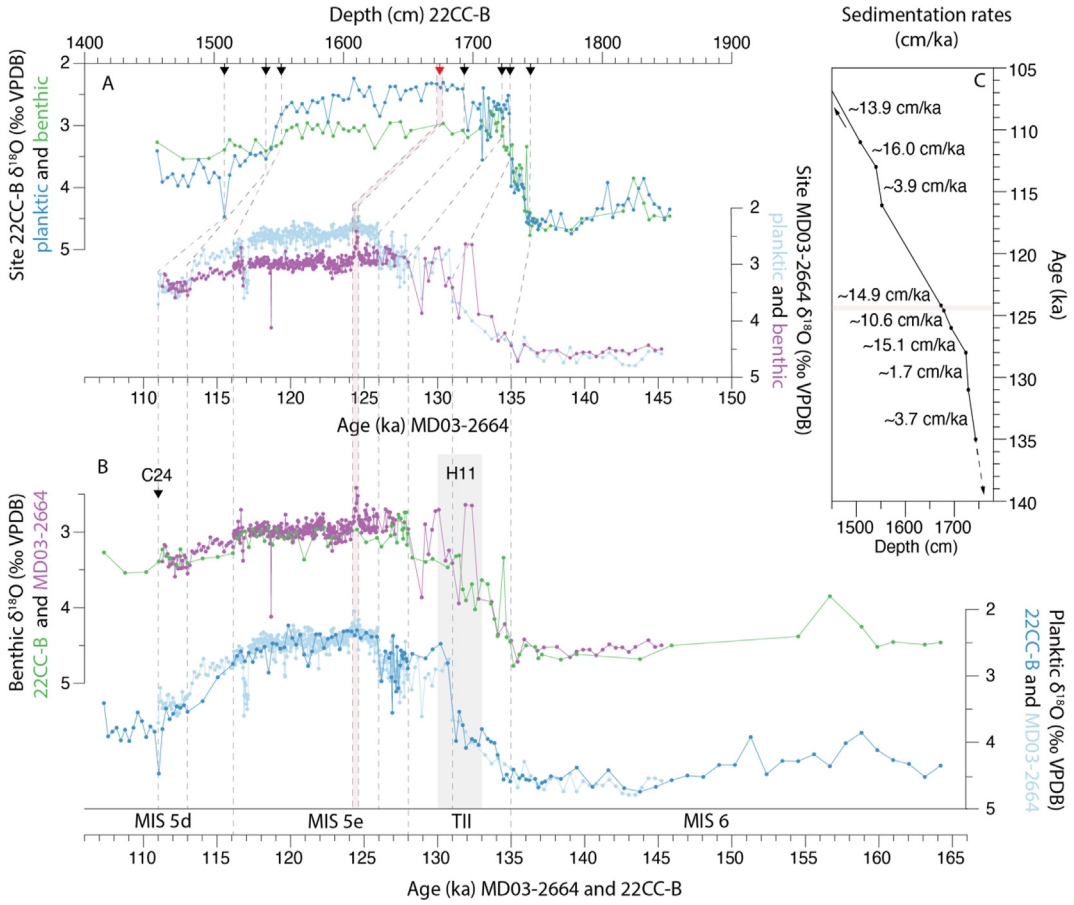

Fig. 2. Age model for Core 22CC-B. A) Core 22CC-B planktic and benthic $\delta^{18}O$ plotted on depth, and Core MD03-2664 planktic and benthic $\delta^{18}O$ record plotted on age (ka) (Irvali et al., 2012, 2016). B) Benthic $\delta^{18}O$ of Cores 22CC-B and MD03-2664 plotted on the age scale (ka) of MD03-2664 with the tie points (dashed lines), and planktic $\delta^{18}O$ of Cores 22CC-B and MD03-2664 plotted on age (ka). The red layer is represented by the red arrow and pink shaded area. The grey shaded area represents H11 within TII. C) Depth (cm) versus age (ka) plot for Core 22CC-B, showing tie points and approximate sedimentation rates. The red layer is represented in the pink shaded area.

1998). We identified these MIS 5e boundaries at 22CC-B in our benthic $\delta^{18}O$ record, as well as the onset of Termination II (TII) at the top of MIS 6 (135 ka) and the base of MIS 5d (113 ka) (Fig. 2A).

Additional tie points in our age model are based on the planktic $\delta^{18}O$ record and colour scan. We associate one planktic $\delta^{18}O$ tie point with the distinct isotopic minimum during TII at 131 ka during Henrich event 11 (H11) (Irvali et al., 2016). An abrupt shift in planktic $\delta^{18}O$ recognised in Core 22CC-B and also in Cores MD95-2042 and MD03-2664 (Shackleton et al., 2002, 2003; Irvali et al., 2012) provides an additional tie point at 126 ka (Fig. 2B), that is associated with the start of the Eemian interglacial on land (Shackleton et al., 2003). A distinct "red layer" was observed in both Core 22CC-B and MD03-2664 based on sediment colour properties (Supplementary Fig. 1). The top and bottom of this layer were used as tie points for our age model with the ages of 124.2 and 124.6 ka, respectively (Galaasen et al., 2014). A similar red layer is also documented at the Integrated Ocean Drilling Program (IODP) Site U1305 on the Eirik Drift and was likely deposited by an outburst flood event associated with the final collapse of the Laurentide Ice Sheet (LIS) in the early part of the LIG (Nicholl et al., 2012). The final tie point is placed at the rapid increase of planktic $\delta^{18}O$ at 111.0 ka in MIS 5d (Fig. 2B), which corresponds in Core MD03-2664 to a large IRD peak reflecting the C24 event (e.g. Hodell et al., 2009). In summary, our age model utilizes the same tie points that Irvali et al. (2012, 2016) and Galaasen et al. (2014) used to correlate their record to MD95-2042 of Shackleton et al. (2002, 2003). Additionally, in order to have some control on the ages of the upper MIS 5d, i.e. younger than 111 ka, we used a ^{14}C AMS age from a twin core on the Eirik Drift (46 ka at 602.7 cm core depth in hole 22CC-A; Griem et al., 2019). We transferred the ^{14}C age from Core 22CC-A to 22CC-B by aligning the red-green colour scan and magnetic susceptibility. The ages <111 ka are thus approximate and should not be considered as absolute ages. The base of MIS 6 is not constrained, and the ages >135 ka are based on a linear extrapolation of the sedimentation rate between 131 and 135 ka. Thus, the ages of an extended MIS 6 beyond 135 ka are imprecise and should be used cautiously.

4.2. Isotopes

The late MIS 6 planktic (*N. pachyderma* sinistral) and benthic (*C. wuellerstorfi*) $\delta^{18}O$ show typical glacial values of, on average, ~4.4‰ and ~4.5‰, respectively (Fig. 2B). From ~135 ka, both benthic and planktic $\delta^{18}O$ shift towards lower values, marking the initiation of TII. Within TII, the planktic $\delta^{18}O$ decreases from 4.0 to 2.7‰ at 131 ka, associated with H11. The onset of the MIS 5e low benthic $\delta^{18}O$ plateau at 128.0 ka is characterised by an increase in sedimentation rate from 1.7 cm/ka to 15.1 cm/ka (Fig. 2C). The lowest benthic $\delta^{18}O$ values occur between 128 and 126.5 ka. In this same period, the planktic $\delta^{18}O$ shows high variability, ending in a distinct increase at ~126.5 ka, followed directly by a decrease of 0.7‰. From the middle to late MIS 5e, the benthic and planktic $\delta^{18}O$ are

consistent with characteristic low values of interglacial periods. Both isotopic records show a general increasing trend throughout MIS 5e. The transition into MIS 5d is characterised by a gradual increase in planktic $\delta^{18}O$, and a more muted increase in benthic $\delta^{18}O$, suggesting a change in local surface water hydrography in excess of the change registered in the deep ocean.

4.3. Dinoflagellate cysts

In MIS 6 dinocyst counts (Fig. 3) are very low making reliable interpretations based on relative abundance difficult. Towards TII, concentrations are also very low (average of ~27 cysts/g sediment), yet they increase to an average of 110 cyst/g sediment. Here, we observe the onset and increase in the relative abundance of RBC which during TII reach up to ~30% of the dinocyst assemblage.

The dinocyst concentration increases at the onset of MIS 5e (Fig. 3A). *Spiniferites* spp., RBC, cysts of *P. dalei* and *N. labyrinthus* are among the species that contribute to the concentration increase (Fig. 3F–I). RBC reach, at maximum, 30% of the total assemblage in the earliest MIS 5e (128–126.5 ka). At 126.5 ka, the abundance and concentrations of RBC rapidly decrease and *B. tepikiense* becomes the dominant species (60%) (Fig. 3E).

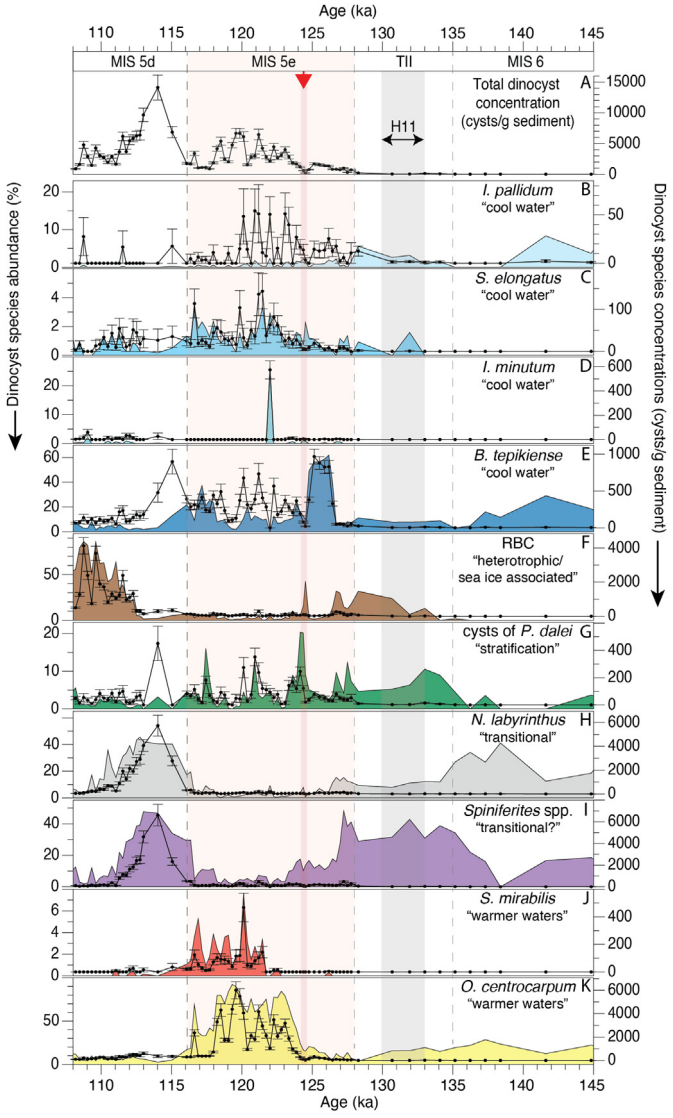

Fig. 3. Dinocyst relative abundances (%) represented with coloured curves and concentrations (cyst/g sediment) with errors represented with black lines for the most abundant species of Site 22CC-B plotted on age (ka). A) The total dinocyst concentration with errors, B–K) relative abundance and concentration with errors. The red shaded area and arrow represent the red layer. The grey shaded area represents H11, and the pink shaded area marks MIS 5e.

The "red layer" event (124.6–124.2 ka) is reflected by a decrease of dinocyst concentrations and marks the onset of a different dinocyst assemblage. *B. tepikiense* is first replaced at the "red layer" by the heterotrophic group of RBC (43%) and thereafter cysts of *P. dalei* (20%). Other noteworthy dinocyst taxa in the "red layer' include the cyst of *Scrippsiella trifida* which appears almost exclusively here. Shortly following the deposition of the red layer and cysts of *P. dalei*, overall cyst concentrations rise. In addition, the relative abundance of *O. centrocarpum* increases to an average of ~72%, while its concentration increases to maximum values and fluctuates between ~1000 and 5000 cyst/g sediment for the next 6000 years (Fig. 3K). In this interval, we also encounter the warm water indicator *S. mirabilis* between 121.5 and 115 ka (Fig. 3J). In a single sample (~122 ka), we encountered high relative abundances of the Arctic, cool water dinocyst *Islandinium minutum*, a species often associated with sea ice (Fig. 3D). Other sea ice proxies (see section 3.3) were not recorded associated with this sample. *O. centrocarpum* concentrations and abundances decrease at ~118 ka, when *B. tepikiense* and cysts of *P. dalei* increase.

The MIS 5d dinocyst assemblage is initially dominated by *N. labyrinthus* and *Spiniferites* spp., together representing up to 90% of the assemblage at its maximum. The dominance of these species corresponds with the highest overall dinocyst concentrations of the record reaching a maximum of 14,000 cyst/g sediment. When *N. labyrinthus*, *Spiniferites* spp., and dinocyst concentrations decrease at ~114 ka, RBC start dominating the assemblage for the remainder of MIS 5d.

4.4. Biomarkers

Through MIS 6, the sea ice (IP_{25}, HBI II) and MIZ (HBI III Z) HBI biomarkers are low or under the detection limit while the open ocean (brassicasterol, dinosterol) and terrestrial (sitosterol and campesterol) sterol biomarkers are low in concentration (Fig. 4D–G). In late TII all biomarkers, and especially the HBI biomarkers, increase in concentrations corresponding to the abrupt transition to the lower planktic $\delta^{18}O$ values at 131 ka. At the onset of MIS 5e (128 ka), all biomarker concentrations rapidly increase further with IP_{25} and HBI II reaching maximum values between 127.4 and 126.9 ka. Maximum values of HBI III (Z), brassicasterol, dinosterol, sitosterol, and campesterol remain until ~126.4 ka. Subsequently, all biomarker concentrations decrease from 126.4 ka, only to briefly increase in the red layer. Here, the sea ice and other biomarkers peak except for HBI III (Z), and we record the highest concentration of the terrestrial biomarker sitosterol at 49 μg/gTOC in this red layer. For the remainder of MIS 5e, all biomarker concentrations decline and sea ice biomarkers are not detected. At the start of MIS 5d, the biomarker concentrations increase and IP_{25} is detected again from ~114 ka and remains present throughout MIS 5d.

5. Discussion

5.1. Late MIS 6 and Termination II: the perennial sea ice cover breaks up

During our studied interval of MIS 6, the Eirik Drift was likely covered by an extensive perennial sea ice cover. This interpretation is based on the very low dinocyst concentrations (Fig. 4A) and low to absent IP_{25} concentrations in our samples (Fig. 5E). IP_{25}

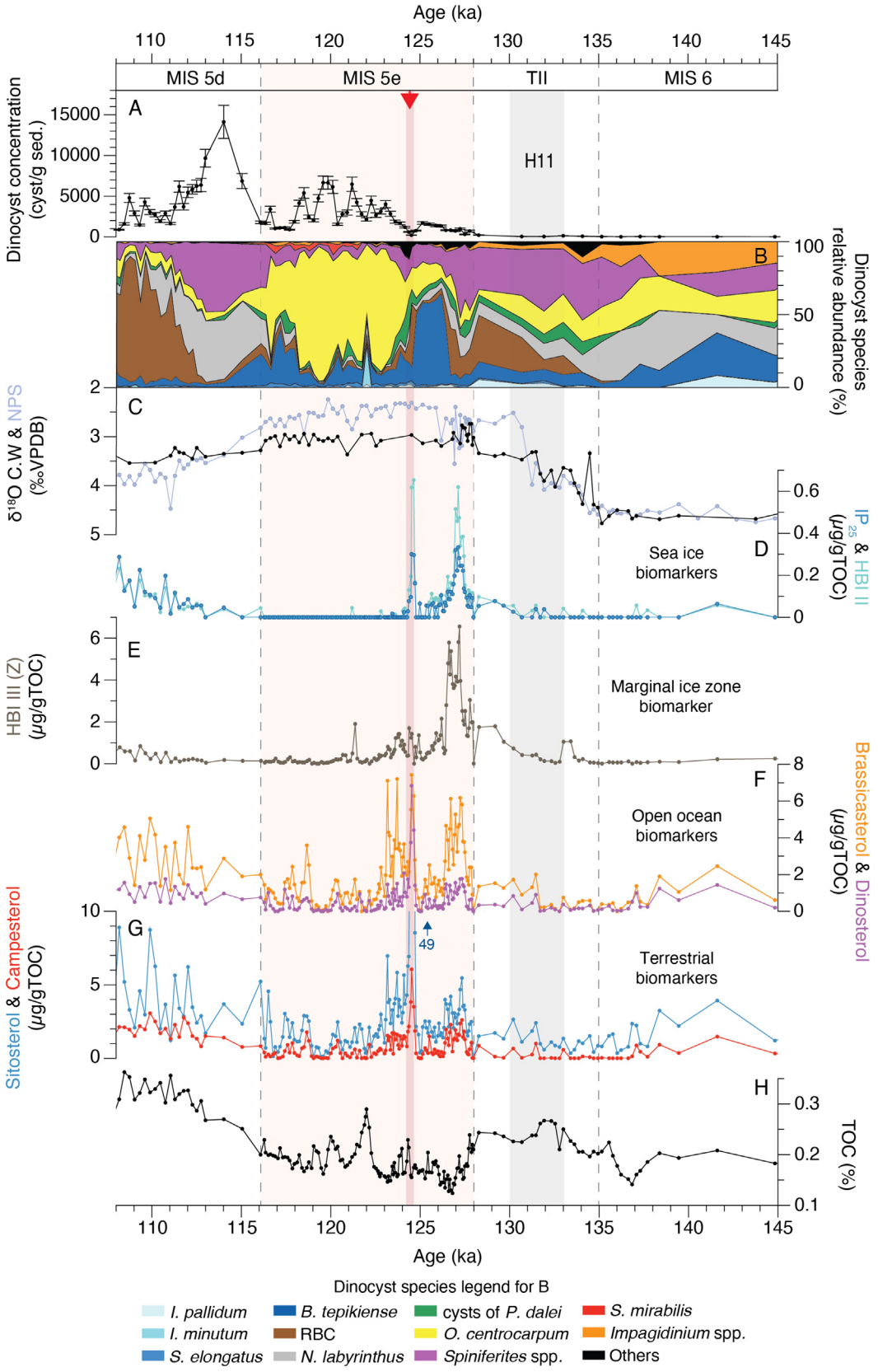

Fig. 4. Dinocyst, stable oxygen isotope, and biomarker results plotted on age (ka). A) Dinocyst total concentrations with errors, B) dinocyst species relative abundances, C) $\delta^{18}O$ of *C. wuellerstorfi* and *N. pachyderma* (s), D) concentrations of sea ice and sea ice associated biomarkers IP_{25} and HBI II, E) concentration of the marginal ice zone biomarker HBI III (Z), F) concentrations of the open ocean biomarkers brassicasterol and dinosterol, G) concentrations of the terrestrial biomarkers sitosterol and campesterol and H) TOC %. The red shaded area and arrow represent the red layer. The grey shaded area represents H11, and the pink shaded area marks MIS 5e.

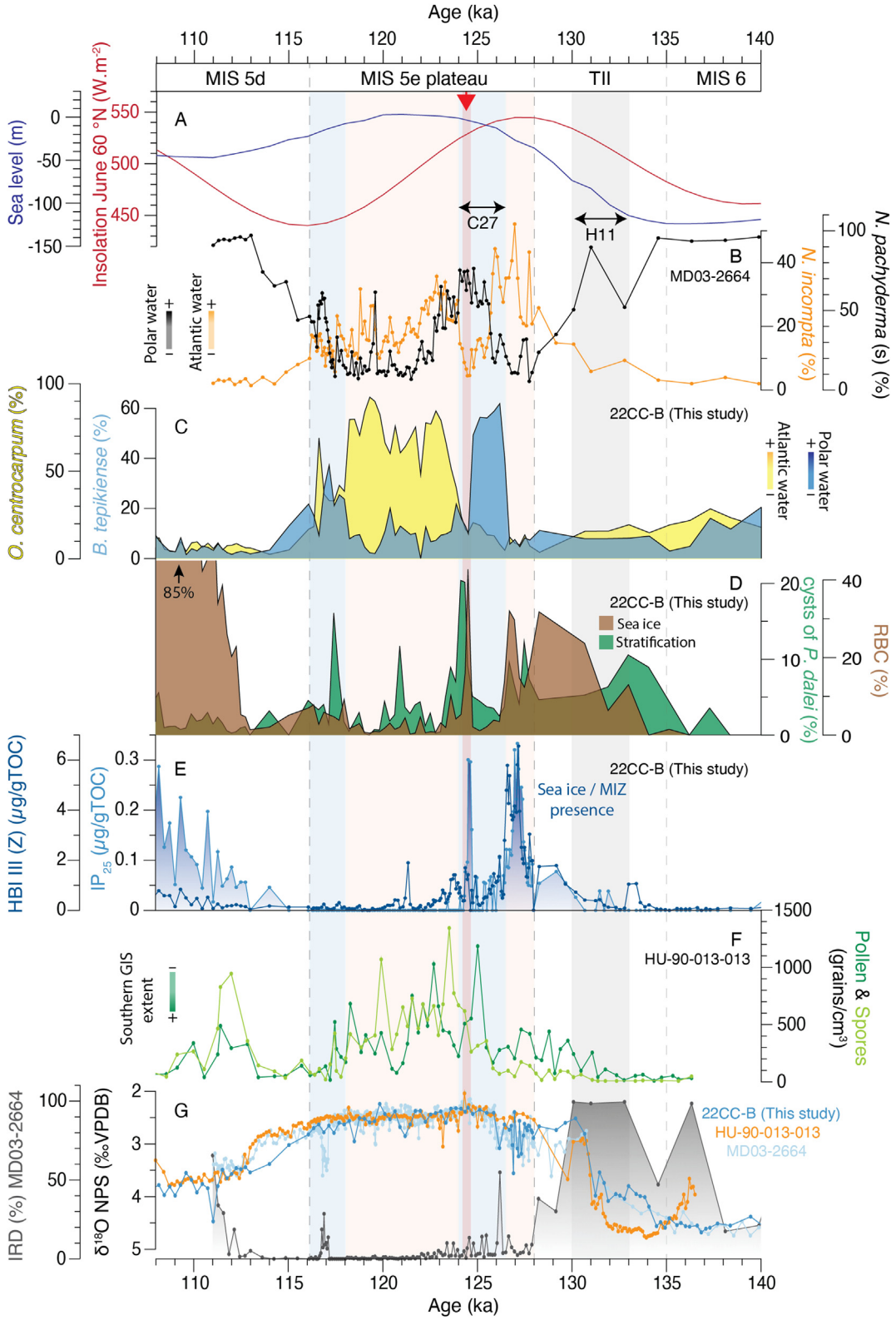

Fig. 5. A) June insolation at 60°N (Berger and Loutre, 1991) and sea level in meters relative to modern (Spratt and Lisiecki, 2016), B) relative abundance of the cold water *N. pachyderma* (s) and the Atlantic water indicator *N. incompta* from Core MD03-2664 (Irvali et al., 2012, 2016), C) relative abundance of *O. centrocarpum* and *B. tepikiense* from Core 22CC-B, D) relative abundance of the round brown cysts (RBC), an indicator for high nutrient availability and sea ice, and cysts of *P. dalei* which are often linked to stratified waters, E) concentrations of the sea ice (IP_{25}) and marginal ice zone (HBI III (Z)) biomarker, F) pollen and spore records from Core HU-90-013-013 and estimated ice cover on Greenland (de Vernal and Hillaire-Marcel, 2008), G) Eirik Drift planktic foraminifer $\delta^{18}O$ records, and IRD from Core MD03-2664 (black). The Heinrich Event 11 (H11) is marked by the grey shaded area. Periods within MIS 5e characterised by warm water inflow to the Eirik Drift via the Irminger Current (IC) are marked by the pink shaded area; the cold event C27 and the cooler conditions with enhanced pulses of EGC at the end of MIS 5e are marked by the blue shaded areas. The red layer is marked by the red arrow and red shaded area.

concentrations of (almost) zero can reflect open water conditions but combined with low open water biomarkers (brassicasterol, dinosterol, and HBI III (Z)), we interpret these records to reflect a perennial sea ice cover with minimal open-water phytoplankton production. A thick sea ice cover limits light penetration in the surface ocean and nutrient availability, both of which are essential for phytoplankton and sea ice algae productivity (Müller et al., 2011; Fahl and Stein, 2012; Xiao et al., 2015). The Core MD03-2664 foraminifer assemblage and stable isotopes have been interpreted to reflect an extended sea ice margin occurring south of our core location and increased polar water influence via the EGC (Irvali et al., 2012). However, the low but present dinocysts and biomarkers and the infrequent occurrence of foraminifers at Site 22CC-B may suggest that the perennial sea ice cover was interrupted by short intervals with restricted open water conditions during summer that allowed phytoplankton reproduction. Indeed, Mokeddem and McManus (2016) demonstrate with foraminifer records from the Ocean Drilling Program (ODP) Site 984 that a baseline of full glacial conditions was interrupted by short-lived retreats of the polar front northward that allowed warm and saline water inflow to the northwest Atlantic.

At the onset of TII the perennial sea ice likely started to break up more frequently when summer insolation increased (Fig. 5A). The dinocyst counts and concentrations are very low (Fig. 3), yet the relative abundances are statistically significant, as determined using the method of Heslop et al. (2011) (Supplementary Fig. 2). RBC, a group of heterotrophic dinocysts often associated with seasonal sea ice, occur for the first time in our record and increase in relative abundance. At ~130 ka, as local summer insolation neared its peak, the perennial sea ice broke up more frequently and we record increased IP_{25} and HBI III (Z) concentrations. The sea ice was still extensive but less so than in MIS 6 and early TII. A drop in IRD % (Fig. 5G) and in the abundance of polar foraminifers in Core MD03-2664 at 130 ka (Fig. 5B) suggests a general retreat of polar conditions as TII came to an end.

The dinocyst assemblage at the Eirik Drift shows no indications of Atlantic water inflow during TII, similar to the assemblage from the South Icelandic Basin Core MD95-2015 (Eynaud et al., 2004). In contrast, the Nordic Seas were influenced by warm Atlantic water, as indicated by the dominance of the Atlantic water tracer *O. centrocarpum* at the Vøring Plateau (Core M23071; Van Nieuwenhove et al., 2008). Together, this could point to a contracted SPG to the west. A contracted or weakened SPG would allow for warm and saline Atlantic waters to flow northward into the Nordic Seas, while the western North Atlantic is cut off from warm water inflow (Hátún et al., 2005; Thornalley et al., 2009; Bauch et al., 1999, 2012; Van Nieuwenhove et al., 2011). Such a scenario of a contracted or weakened SPG is also proposed by Zhuravleva et al. (2017) who indicate cold surface water conditions, high meltwater input from the GIS and/or enhanced sea ice in East Greenland Margin Core M23351. Taken together, the break-up of perennial sea ice, and a highly fresh and stratified upper ocean in the North Atlantic is consistent with a contracted/weak SPG during TII (Fig. 6).

5.2. MIS 5e

5.2.1. Earliest MIS 5e (128–126.5 ka): marginal ice zone and (sub) surface warming

Coincident with peak summer insolation in the earliest MIS 5e, we record the first evidence of a MIZ at the Eirik Drift. We interpret a MIZ due to the simultaneous increase of the sea ice biomarkers IP_{25} and HBI III (Z) (Fig. 5E). While IP_{25} alone could indicate sea ice transport via the EGC, HBI III (Z) is found to be strongly enhanced in MIZ environments in the Antarctic (Collins et al., 2013) and the Arctic (Belt et al., 2015). Further corroborating evidence for MIZ conditions comes from increased concentrations and abundances of the heterotrophic RBC, which are often abundant in highly productive sea ice environments (e.g. de Vernal et al., 1997, 2005, 2020), and cysts of *P. dalei*, a species associated with stratified waters (Fig. 5D; see section 3.3). Contemporaneously, sea surface productivity increased as indicated by the open-water phytoplankton biomarkers dinosterol and, especially, brassicasterol (Fig. 4F). The environment during the first 1500 years of MIS 5e at the Eirik Drift was thus an environment with sea ice, high productivity and stratification.

Interestingly, several data records and modelling experiments highlight this earliest part of MIS 5e to be the warmest part of the entire interglacial. Foraminifer-based temperature reconstructions from Core MD03-2664 demonstrate peak MIS 5e temperatures at the Eirik Drift (Irvali et al., 2012). Furthermore, in Core MD03-2664, the shift in the foraminifer assemblage from dominance of *N. pachyderma* (s) during MIS 6/TII to an assemblage with the subpolar-transitional species *N. incompta* (Fig. 5B), and *T. quinqueloba*, *G. bulloides* and *G. glutinata*, suggest an increased Atlantic water influence (Irvali et al., 2012). Similarly, foraminifer records from Core HU-90-013-013 on the Eirik Drift (Seidenkrantz et al., 1995, 1996), ODP 984 south of Iceland (Mokeddem et al., 2014) and isotope records from IODP Site U1304 on the Gardar Drift (Hodell et al., 2009) point to early MIS 5e warmth and provide broad evidence for warm Atlantic waters. Peak early MIS 5e warmth is further corroborated by several model experiments (e.g. Otto-Bliesner et al., 2006; Bakker et al., 2014). The higher surface ocean temperatures at the Eirik Drift are likely related to an active and west-east oriented SPG drawing in water from the IC as it does today (Fig. 6; e.g. Irvali et al., 2012, 2016; Bauch et al., 2011). This potentially zonally extended SPG configuration appears to have coincided with active dense water formation and ventilation in the Nordic Seas. This is evidenced by high values of benthic carbon isotopes on the Eirik Drift where the deep waters are influenced by the dense overflows from the Nordic Seas (Galaasen et al., 2014). Thus, in this scenario, a seemingly extended SPG is related to a strong AMOC, or at least well-ventilated dense overflows from the Nordic Seas, and not a weak AMOC as suggested by Klockmann et al. (2020). This highlights the complexity of the interaction between SPG dynamics and North Atlantic circulation, and that SPG geometry and strength are by no means the sole modulator of Nordic Seas ventilation.

Taken at face value, it seems difficult to reconcile a MIZ with peak warm MIS 5e near-surface ocean conditions. Discrepancies between reconstructions with different proxies are not uncommon, and have been linked to both habitat difference (i.e. water depth) and/or seasonality (e.g. de Vernal et al., 2020; Van Nieuwenhove et al., 2016; Andersson et al., 2010; Cortese et al., 2005; Risebrobakken et al., 2011; Leduc et al., 2010). Here, taking the habitat into account, biomarkers and dinocysts likely record changes in the uppermost part of the water column, where cold, sea ice laden surface waters occur. The planktic foraminifers would occupy the slightly deeper, warmer waters sourced by the IC. It is well known that planktic foraminifers occur in a sub-surface, slightly deeper habitat (e.g. Simstich et al., 2003; Kozdon et al., 2009; Jonkers et al., 2010; Pados and Spielhagen, 2014). Alternatively, the proxies reflect different seasons, with biomarkers/dinocysts reflecting more spring and autumn conditions and the planktic foraminifers reflecting the summer. For this reason, caution must always be taken when looking at a single proxy. Assuming that the subsurface habitat of *N. pachyderma* (s) also reflects surface ocean conditions, can lead to misinterpretation under some circumstances as pointed out by e.g. Hillaire-Marcel et al. (1994) and Dokken et al. (2013). Indeed, the subsurface

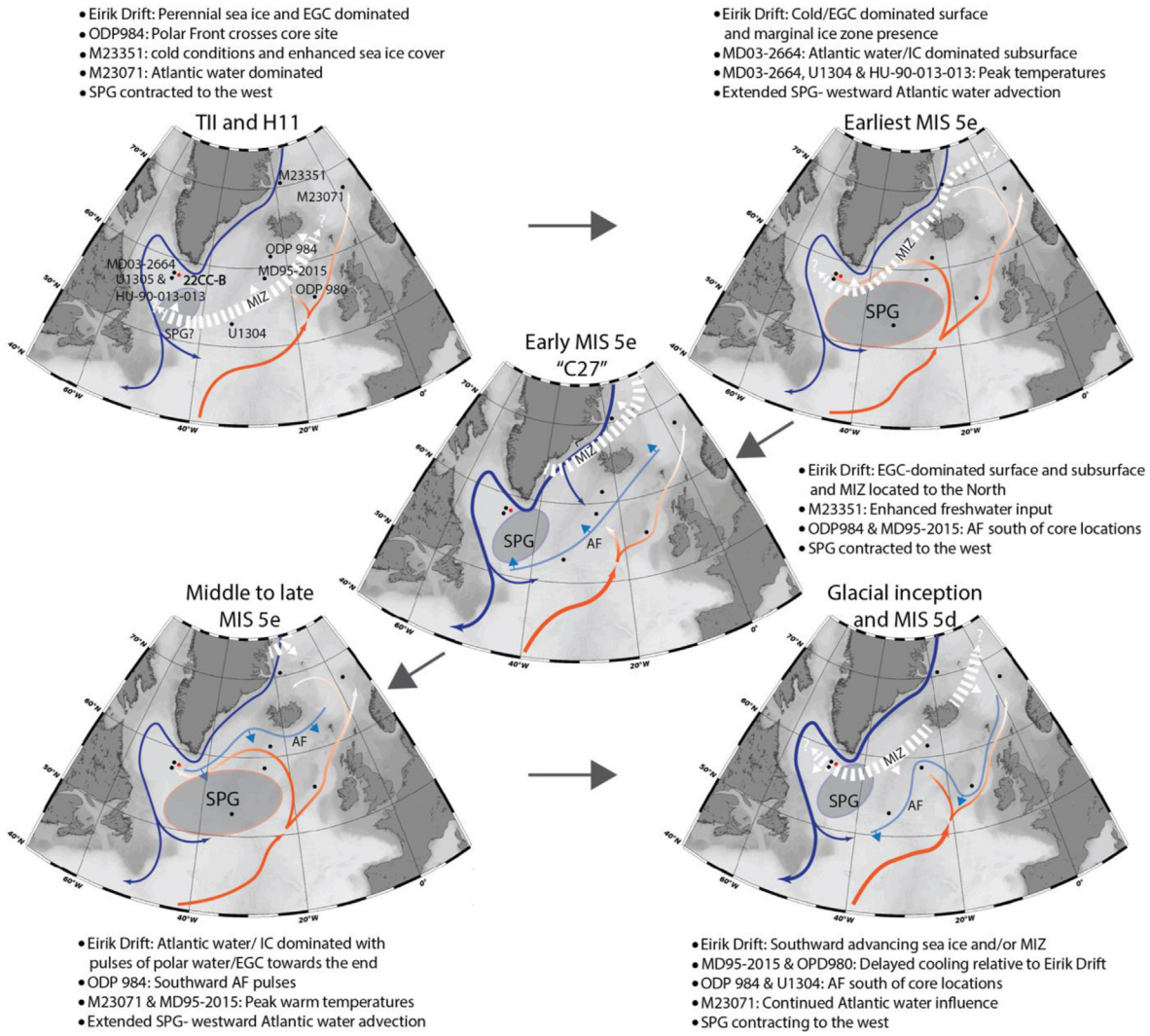

Fig. 6. Schematic North Atlantic surface hydrography during the late TII and H11, MIS 5e, and the last glacial inception and early MIS 5d. Surface ocean currents are indicated by dark blue (polar waters) and orange arrows (Atlantic waters). Thicker blue lines (polar water) mark periods with increased EGC dominance and potential increased freshwater by rerouting. The most likely position during each of the time intervals of the marginal ice zone (MIZ; white dashed lines), the Arctic Front (AF; light blue lines), and the subpolar gyre (SPG; grey shaded circles) are shown. The retreat or advance of the AF and MIZ are indicated by arrows.

habitat of *N. pachyderma* (s) may be particularly well-suited for recording warming events in the subsurface during episodes of stratification and surface cooling (e.g. Max et al., 2022). Viewed in this light, the warm foraminifer-based temperatures of the early MIS 5e could be caused by warm Atlantic waters circulating beneath a fresh surface layer and sea ice. This is similar to what occurs today when warm Atlantic water meets, and subducts beneath, fresh polar water in regions where a strong halocline is maintained by sea ice (Rudels et al., 2015). The presence of sea ice would, in turn, hinder ocean to atmosphere heat flux and cooling locally, potentially further contributing to a warm subsurface IC.

We speculate whether the MIZ location in the Labrador Sea could have played a role in maintaining or strengthening the SPG circulation and influenced the transport of warm and saline waters to the Eirik Drift. Although sea ice can inhibit local deep water formation, its proximity to the Labrador Sea convection regions may have stimulated heat and buoyancy loss, and therefore dense water formation that would affect the SPG strength. Near the polar MIZ today, Cold Air Outbreaks (CAOs) occur where strong winds off the sea ice edge play an important role for water mass transformation (Smedsrud et al., 2022). Thus, a MIZ immediately north of convection regions in the Labrador Sea might have stimulated water mass transformation in the subpolar region, altering the density structure and strength of the SPG (Born and Stocker, 2014). While more data will be necessary to test this concept, if correct, it could point to the MIZ being a critical factor to invigorate or maintain the SPG circulation during the earliest MIS 5e. Independent of the actual gyre configuration, our data indicate that when a MIZ was present at the northern margin of the SPG, a relatively cool surface and a halocline was maintained over a warmer subsurface layer of Atlantic Water (IC origin) at peak summer insolation. By analogy with today's Arctic, where similar configurations exist where Atlantic Water meets the sea ice edge (e.g. Årthun et al., 2012; Rudels et al., 2015), the presence of sea ice may have been a critical factor in maintaining this mode of stratification.

5.2.2. Early MIS 5e (126.5–124 ka): hydrographic shift and subsurface cooling

The surface ocean hydrography profoundly shifted at ~126.5 ka and the influence of Atlantic water to the subsurface was replaced by a stronger EGC influence. At the same time, the MIZ retreated north, away from the Eirik Drift. The EGC influence is inferred from

the rapid increase in abundance of the polar front associated dinocyst, *B. tepikiense* (Fig. 5C). IP_{25} concentrations decrease considerably, reflecting reductions in spring sea ice cover. However, HBI III (Z), HBI II, and IP_{25} do remain present in several samples, indicating the occasional occurrence of sea ice in the area (Fig. 5E). Cold, stratified surface waters characterised by large seasonal temperature variations and occasional sea ice cover is consistent with the high abundance of *B. tepikiense* (de Vernal et al., 2005, 2020) that is recorded here and similarly in the South Icelandic Basin (Eynaud et al., 2004). Seasonally open waters with increased sea surface productivity are recorded on the East Greenland margin which suggests a MIZ retreat far north of the Eirik Drift (Zhuravleva et al., 2017). At the Eirik Drift the foraminifer assemblage changes from a dominance of *N. incompta* to *N. pachyderma* (s) (Fig. 5B; Core MD03-2664; Irvali et al., 2012). This is also observed in Core HU-90-013-013 (Seidenkrantz et al., 1995) and suggests that Atlantic water influence decreased and cooler EGC conditions dominated.

This increasing EGC influence occurs during the C27 cooling event that is recognised in several North Atlantic proxy records (e.g. Oppo et al., 2006; Mokeddem et al., 2014; Irvali et al., 2016; Mokeddem and McManus, 2016; Tzedakis et al., 2018). A cooling event around this time is also observed in numerous locations across the North Atlantic and has been described as "stepwise deglaciation" or "reversal in deglacial warming trend" (e.g. Seidenkrantz et al., 1995, 1996; Risebrobakken et al., 2006; Bauch and Erlenkeuser, 2008; Van Nieuwenhove et al., 2011; Bauch et al., 2011, 2012; Zhuravleva et al., 2017).

In the light of this widespread North Atlantic cooling, it may seem incongruous that we record a northward retreat and decline in sea ice at the Eirik Drift. Sea ice retreat, despite continued polar water export, may simply be due to high summer insolation (Fig. 5A) and atmospheric CO_2 (Lüthi et al., 2008) at the time, which would have made it hard for sea ice to survive at the Eirik Drift, even in a cool surface ocean. Indeed, despite the evidence of cooler conditions and enhanced EGC in the early MIS 5e, the conditions on Greenland itself were mild. On the Eirik Drift (Core HU-90-013-013), de Vernal and Hillaire-Marcel (2008) show increased pollen and spore concentrations indicating a rapid expansion of vegetation in southern Greenland (Fig. 5F) and implying a retreat of the GIS. Simultaneously, intensified melting from the northeastern GIS is demonstrated by the isotopic record of Core M23351 (Zhuravleva et al., 2017) and sediment chemistry (Carlson et al., 2008; Colville et al., 2011), consistent with a widespread cryospheric decline at this time.

It has been proposed that increased freshwater input from a melting GIS and/or sea ice is a driving mechanism behind surface ocean cooling and changes in SPG circulation during the early LIG (e.g. Irvali et al., 2012, 2016; Mokeddem et al., 2014; Galaasen et al., 2014; Tzedakis et al., 2018). According to model simulations (Born et al., 2010), increased freshwater input to the Labrador Sea could weaken the SPG by altering the surface water salinity and density, and the rate of dense water formation in the Labrador Sea. It has been suggested that a weakened and contracted SPG (Fig. 6) allows for warmer subtropical waters to penetrate farther to the northeast and into the Nordic Seas (Hátún et al., 2005; Thornalley et al., 2009; Bauch et al., 1999, 2012; Van Nieuwenhove et al., 2011) invigorating deep water formation in the Nordic Seas, while Atlantic water transport westward to the Labrador Sea decreases. While such a shift in gyre dynamics could help explain the reduced input of IC water to the Eirik Drift at this time and the prevalence of cold, fresh, polar-like conditions, it does not readily explain the coeval decrease in deep water ventilation at the site. Deep water formation in the Nordic Seas seems to have been weakened during this time, as evidenced in depleted benthic $\delta^{13}C$ values on the Eirik Drift (Galaasen et al., 2014), since this site is influenced today by dense (Denmark Strait) overflow waters. Supporting a reduced ventilation of Nordic Seas deep water at this time, low $\delta^{13}C$ values have been recorded around 126.5 ka on the East Greenland margin (Zhuravleva et al., 2017) and in the Nordic Seas (Bauch et al., 2012). Although the Nordic Seas depletions appear smaller and shorter (~1000 years) compared to the Labrador Sea (~2500 years), they first occur together with the C27 cooling phase.

Another factor contributing to increasing EGC and polar-like conditions could be the potential rerouting of freshwater caused by the presence of an ice sheet over the Canadian Arctic Archipelago (CAA; Condron and Winsor, 2012; Lofverstrom et al., 2022). As sea level rose coming out of the glacial period and the Bering Strait opened, freshwater could once again flow from the Pacific to the Atlantic via the Arctic Ocean. If a remnant LIS remained in the CAA, all freshwater that today can flow freely through the Davis Strait west of Greenland would be rerouted through the Fram Strait, into the EGC and onwards into the North Atlantic deep convection regions. Previous studies have also shown that AMOC strength and North Atlantic climate is sensitive to the status of gateways in the Arctic (Otto-Bliesner et al., 2006; Hu et al., 2010; Karami et al., 2021). We hypothesise that Arctic rerouting of Pacific freshwater remains a potential contributor to the enhanced influence of the relatively cool and fresh EGC in the early MIS 5e. Condron and Winsor (2012) and Lofverstrom et al. (2022) suggest such rerouting as a potential feedback mechanism behind the Younger Dryas cooling late in the last deglaciation. Interestingly, the C27 event associated with the EGC expansion south of Greenland and the surface ocean cooling in the North Atlantic, have often been compared to the Younger Dryas (e.g. Sarnthein and Tiedemann, 1990; Seidenkrantz et al., 1996; Sánchez Goñi et al., 2005). Two prerequisites are necessary for this EGC focused freshwater routing to be plausible. One, sea level must have been high enough for the Bering Strait to be open, and two, enough glacial ice must have persisted to block freshwater export routes west of Greenland (Lofverstrom et al., 2022). The first condition seems to have been met: sea level was high enough during this period (Fig. 5A; Spratt and Lisiecki, 2016) to allow freshwater transport across Bering Strait. For the second condition to be met, the LIS must have remained sufficiently large early in MIS 5e to have blocked freshwater export through the CAA, despite the orbitally modulated high summer insolation.

An interesting sedimentological feature in our core is the red layer at the end of the C27 cooling. It is associated with a sudden rapid re-occurrence of sea ice at the Eirik Drift which is distinctly marked by the occurrence of IP_{25}, and RBC, followed by cysts of *P. dalei*. Taken together they indicate a short event of rapid sea ice discharge, meltwater and stratification. This signal was likely transported and does not represent a reappearance of the MIZ at our site, which is further supported by the low MIZ marker HBI III (Z). Furthermore, cysts of *S. trifida* have been linked to LIS-sourced meltwater input around southern Greenland and south-eastern Canada for early Holocene sediments (Head et al., 2006; Van Nieuwenhove et al., 2018), and its occurrence here in the LIG may equally suggest an origin from Canadian waters. The red layer found in our core, and in Cores MD03−2664 and U1304, has been linked to an outburst flood event through the Hudson Strait (Nicholl et al., 2012; Shaw and Lesemann, 2003) akin to the 8.2 ka event early in the Holocene when the southern margin of the LIS retreated enough that proglacial lake Agassiz broke through the ice dam blocking its drainage through Hudson Straight (Hillaire-Marcel et al., 2007) and deposited a similar red layer (Kerwin, 1996; St-Onge and Lajeunesse, 2007; Lajeunesse and St-Onge, 2008). The similarity between the sediment deposits and their relative timings, early in both interglacials, suggests similar mechanisms behind the events. This implies that like during the Holocene, there

could have been a residual LIS presence even after peak summer insolation during early MIS 5e. Such a remnant large ice mass would be consistent with the recent suggestion of an early MIS 5e sea level high stand related to Antarctic melting, whereas the GIS contribution rather played a larger role later in MIS 5e (Rohling et al., 2019). Regarding the freshwater rerouting theory, a remnant LIS could hint that ice cap remnants occurred also further north in the CAA; however this remains indirect, inconclusive evidence that ice restricted or blocked the CAA freshwater route.

5.2.3. Middle to late MIS 5e (124–116 ka): Atlantic water advection and occasional cold-water events

For the remainder of MIS 5e, the surface waters at the Eirik Drift are characterised mainly by Atlantic water inflow via the IC and an extended and/or strong SPG. This is evident from the dominance of the Atlantic water indicator *O. centrocarpum* and the absence of sea ice biomarkers, demonstrating open waters. From ca. 122 ka, a low but notable and sustained occurrence of *S. mirabilis* (Fig. 3J) indicates warm-temperate waters (see section 3.3). This species characterises interglacial optima in the northern North Atlantic and is known in late MIS 5e from the Gardar Drift (Core MD95-2015; Eynaud et al., 2004), Nordic Seas (Core M23071; Van Nieuwenhove et al., 2008), and even Fram Strait (Van Nieuwenhove et al., 2011). While its occurrence is used to interpret a late glacial optimum for these areas (e.g. Van Nieuwenhove et al., 2011), we find that at the Eirik Drift the influence of warm Atlantic water via the IC was interrupted by episodes of cold Arctic water outflow through the EGC. These intermittent incursions of EGC influence occur against a background of declining sea surface temperature (Irvali et al., 2016) and summer insolation (Fig. 5A). Similar late MIS 5e cooling events have been documented in the central (ODP 984; Mokeddem et al., 2014) and eastern subpolar North Atlantic (ODP 980; Oppo et al., 2006). In our study, peaks of the cysts of *P. dalei* and *B. tepikiense* indicate these incursions of cold water masses and southward pulses of the Arctic Front, especially since *B. tepikiense* is a frontal zone indicator reflecting cold, stratified surface waters characterised by large seasonal temperature variability (de Vernal et al., 2005, 2020). The largest cold water excursions at the Eirik Drift are around 118–117 ka where the cysts of *P. dalei* and *B. tepikiense* increase in abundance, and the Atlantic water indicator *O. centrocarpum* decreases (Fig. 5C and D). In Core MD03-2664, the 117 ka cooling is marked by a peak in IRD, a large anomaly in the planktic oxygen isotopes (Fig. 5G), and an increase in *N. pachyderma* (s) (Fig. 5B; Irvali et al., 2016). These data together reflect enhanced GIS activity and growth, and colder surface ocean conditions towards the end of MIS 5e. Additionally, expanded GIS extent is inferred from a decrease in the pollen and spore concentrations (Fig. 5F; de Vernal and Hillaire-Marcel, 2008) from the Eirik Drift indicating a deterioration of the vegetation in the south of Greenland. On the East Greenland margin short-term, pronounced depletions in both planktic and benthic $\delta^{18}O$ (Core M23351; Zhuravleva et al., 2017) are associated with enhanced freshwater pulses that could be related to the cooling events and increased GIS activity. These cold anomalies indicate that even during the warm LIG, incursions of cold and fresh Arctic water masses influenced the Labrador Sea.

5.3. MIS 5d (116–108 ka): glacial inception and the return of seasonal sea ice

As summer insolation reached a minimum at the transition into MIS 5d, the return of cool conditions led to the return of sea ice at the Eirik Drift. Prior to the return of sea ice, a transitional phase from MIS 5e to 5d is characterised by *N. labyrinthus* and high dinocyst concentrations, indicating increased surface ocean productivity, typically seen at frontal zones. Following the transitional phase, the Arctic front migrated southwards again and EGC-like conditions returned. The EGC likely transported sea ice to the Labrador Sea, as one can interpret from the increased IP_{25} concentrations. The low HBI III (Z) concentrations could suggest that the Eirik Drift is not in the marginal ice zone, however, a readvance of the MIZ towards the Eirik Drift is likely, given the dominance of RBC (Fig. 5D and E).

When examining the North Atlantic on a broader scale, there are differences in the dinocyst assemblages between the western and eastern regions during MIS 5d. While cold conditions are evident at the Eirik Drift, dinocyst assemblages from the southern Icelandic Basin suggest sea ice free conditions and rather warm Atlantic (IC) waters persisted (Core MD95-2015; Eynaud et al., 2004). Furthermore, Eirik Drift sea surface temperature records (Core MD03-2664; Irvali et al., 2016) indicate a larger cooling compared to the central Atlantic ODP 980 (Oppo et al., 2006). The temperature difference and/or delayed cooling response in the east *vs* west is likely explained by the ocean frontal zones, and sea ice expanding south of the Eirik Drift prior to reaching the more eastern site. The frontal zone and/or MIZ was likely located north of the Iceland Basin in a SW-NE orientation, consistent with a weak SPG contracted to the northwest (Fig. 6; e.g. Mokeddem et al., 2014). A contracted SPG allows warmer and more saline water to enter the eastern subpolar North Atlantic and Nordic Seas, while Atlantic water transport via the IC towards the west would decrease (see section 5.2.2). The cooling-fostered return of sea ice could have amplified or even triggered reductions in SPG strength by freshening the surface ocean during the last glacial inception, consistent with model findings (Born et al., 2010). However, it is important to note that the SPG is sensitive not only to buoyancy forcing (e.g. Levermann and Born, 2007; Mengel et al., 2012; Born and Stocker, 2014) but also to atmospheric circulation patterns (e.g. Lohmann et al., 2009).

It is also possible that the glacial inception itself may have played a key role in cooling by influencing pathways of Arctic freshwater and sea ice export to the North Atlantic. Initial ice sheet growth at the last glacial inception was so rapid and substantial that global sea level decreased by as much as 30–50 m between ~120 and 110 ka (Kopp et al., 2009; Spratt and Lisiecki, 2016; Waelbroeck et al., 2002; Lambeck and Chappell, 2001), which is demonstrated by increased IRD at the Eirik Drift (Fig. 5G) and across the North Atlantic (e.g. Risebrobakken et al., 2007; Zhuravleva et al., 2017; Oppo et al., 2006). Lofverstrom et al. (2022) suggested that the low summer insolation at 116 ka was sufficient to grow an ice sheet to once again block the CAA ocean gateways, similar to other modelling studies (Vettoretti and Peltier, 2003; Birch et al., 2017; Born et al., 2010). In addition, the global sea level remained high enough (Fig. 5A) to allow Pacific water inflow through the Bering Strait within the first phase of glacial inception. Similar to what we speculate might have happened in the early MIS 5e (see section 5.2.2), an ice sheet-blocked CAA would have rerouted Arctic freshwater into the EGC, and, via the EGC, south to the Labrador Sea where the increased freshwater could weaken convection and the gyre circulation. Uncertainty remains about whether the potential ice sheet could completely or partly block the CAA due to the depth of the two main export routes, Nares Strait and Lancaster Sound. However, Lofverstrom et al. (2022) argue that due to highly stratified waters in the Nares Strait and Lancaster Sound (Münchow et al., 2015; Prinsenberg and Hamilton, 2005), the formation of a thick floating ice shelf could be sufficient to inhibit freshwater flux through the archipelago. Another challenge is that direct proxy evidence of the ice sheet configuration in the CAA is not available, since ice sheets in later glacial stages have removed evidence of earlier glaciations (Svendsen et al., 2004; Stokes et al., 2012; Batchelor et al., 2019; Kleman et al., 2010; Dalton et al., 2022).

Reliable ice sheet reconstructions in the CAA region and additional evidence of changes in freshwater transport routes are crucial to better evaluate this scenario, and to what extent it ultimately could have impacted the SPG, AMOC and North Atlantic circulation.

6. Summary and conclusions

Based on new sea ice and surface ocean hydrographical data from the Eirik Drift in the Labrador Sea we interpret the paleoceanographic evolution from the penultimate glacial throughout MIS 5e and into MIS 5d as follows.

- MIS 6 (>~135 ka) was characterised by a thick and extensive perennial sea ice cover at the Eirik Drift. The sea ice cover started to break up episodically during TII (135–128 ka), as northern hemisphere summer insolation increased toward its maximum.
- From the onset of MIS 5e (128–126.5 ka), the Eirik Drift surface waters were characterised by a MIZ and the EGC, while the subsurface was influenced by warm Atlantic waters via the IC and an active/extended SPG circulation. It can be hypothesized that the proximity of the MIZ to the Labrador Sea convection regions could have maintained or invigorated SPG circulation during the earliest MIS 5e.
- The MIZ retreated northwards (126.5–124 ka) and both the surface and subsurface were dominated by strong EGC and polar water conditions. High insolation and atmospheric CO_2 probably did not allow for sea ice to survive as far south as the Eirik Drift. This setting is consistent with a weak/contracted SPG circulation coincident with the C27 (cooling) event and/or "deglacial pause" that is observed across the North Atlantic. The interval ended with an outburst flood event, likely from the Hudson Strait region, which is documented by a distinct red layer, and a short-lived surge of sea ice and stratification of the upper water column.
- The second half of MIS 5e (124–116 ka) was characterised by a strong influence (inflow) of Atlantic water via the IC, potentially indicating an extended/strong SPG at this time. This state was interrupted by episodes of cold Arctic water through the EGC, as summer insolation decreased towards the end of MIS 5e.
- At the transition into MIS 5d (116 ka) the Eirik Drift was again dominated by the EGC and a readvance of the Arctic front to the south of the Eirik Drift before sea ice reappeared. The sea ice presence could have played an important role in amplifying the cooling of last glacial inception by diminishing the strength and lateral extension of the SPG.
- We note that intervals of marked increase in EGC influence at both the start (126.5–124 ka) and termination (116 ka) of MIS 5e occur at times when sea level was high enough for the Bering Strait to be open. At the same time, the residual or proto LIS may have been sufficiently expanded to restrict export pathways west of Greenland resulting in a focusing, and intensification of the EGC route for freshwater transport to the SPG. If such a scenario were to be corroborated by future findings, it underlines the possibly important role of cryosphere reconfigurations, and their influence on freshwater export and rerouting to the North Atlantic, for understanding the climate and hydrographic transitions associated with glacial termination and inception.

Finally, our combined dinocyst and biomarker data are the first to unequivocally demonstrate the presence of sea ice during TII, the earliest MIS 5e and MIS 5d as well as indirectly in MIS 6. During the late MIS 5e, cold events were recorded but sea ice was not present as far south as the Eirik Drift. Nevertheless, it appears clear that sea ice played a role in the SPG circulation during glacial termination and inception.

Author contributions

KS and SDS designed the study. KS generated and analysed all data with the help of KF, SDS, RS and USN. USN generated the stable isotope data. KS wrote the manuscript with input from all authors.

Declaration of competing interest

The authors declare that they have no known competing financial interests or personal relationships that could have appeared to influence the work reported in this paper.

Data availability

Raw data is available from www.pangaea.de at https://doi.org/10.1594/PANGAEA.955398

Acknowledgements

This study is part of the AGENSI project, which is funded by the European Research Council (ERC) under the European Union's Horizon 2020 research and innovation program (grant agreement n° 818449). We like to thank the researchers and crew on board RV G.O. Sars during the 2016 cruise of the Ice2Ice project, which was funded by the European Research Council under the European Union's Seventh Framework Programme (FP7/2007–2013, ERC grant agreement n° 610055). We thank Walter Luttmer in the biomarker laboratory, Dag Inge Blindheim for technical support and Malcolm Jones at Palynological Laboratory Service Ltd.

Appendix A. Supplementary data

Supplementary data to this article can be found online at https://doi.org/10.1016/j.quascirev.2023.108198.

References

Andersson, C., Pausata, F.S.R., Jansen, E., Risebrobakken, B., Telford, R.J., 2010. Holocene trends in the foraminifer record from the Norwegian Sea and the North Atlantic Ocean. Clim. Past 6, 179–193.

Årthun, M., Eldevik, T., Smedsrud, L.H., Skagseth, Ø., Ingvaldsen, R.B., 2012. Quantifying the influence of atlantic heat on barents Sea Ice variability and retreat. J. Clim. 25, 4736–4743. https://doi.org/10.1175/JCLI-D-11-00466.1.

Bacon, S., Reverdin, G., Rigor, I.G., Snaith, H.M., 2002. A freshwater jet on the east Greenland shelf. J. Geophys. Res.: Oceans 107. https://doi.org/10.1029/2001JC000935, 5-1-5-16.

Bakker, P., Masson-Delmotte, V., Martrat, B., Charbit, S., Renssen, H., Gröger, M., Krebs-Kanzow, U., Lohmann, G., Lunt, D.J., Pfeiffer, M., Phipps, S.J., Prange, M., Ritz, S.P., Schulz, M., Stenni, B., Stone, E.J., Varma, V., 2014. Temperature trends during the Present and Last Interglacial periods – a multi-model-data comparison. Quat. Sci. Rev. 99, 224–243. https://doi.org/10.1016/j.quascirev.2014.06.031.

Batchelor, C.L., Margold, M., Krapp, M., Murton, D.K., Dalton, A.S., Gibbard, P.L., Stokes, C.R., Murton, J.B., Manica, A., 2019. The configuration of Northern Hemisphere ice sheets through the Quaternary. Nat. Commun. 10, 3713. https://doi.org/10.1038/s41467-019-11601-2.

Bauch, H.A., Erlenkeuser, H., 2008. A "critical" climatic evaluation of last interglacial (MIS 5e) records from the Norwegian Sea. Polar Res. 27, 135–151. https://doi.org/10.3402/polar.v27i2.6172.

Bauch, H.A., Erlenkeuser, H., Fahl, K., Spielhagen, R.F., Weinelt, M.S., Andruleit, H., Henrich, R., 1999. Evidence for a steeper Eemian than Holocene sea surface temperature gradient between Arctic and sub-Arctic regions. Palaeogeogr. Palaeoclimatol. Palaeoecol. 145, 95–117. https://doi.org/10.1016/S0031-0182(98)00104-7.

Bauch, H.A., Kandiano, E.S., Helmke, J., Andersen, N., Rosell-Mele, A., Erlenkeuser, H., 2011. Climatic bisection of the last interglacial warm period in the Polar North Atlantic. Quat. Sci. Rev. 30, 1813–1818. https://doi.org/10.1016/j.quascirev.2011.05.012.

Bauch, H.A., Kandiano, E.S., Helmke, J.P., 2012. Contrasting ocean changes between the subpolar and polar North Atlantic during the past 135 ka. Geophys. Res. Lett. 39. https://doi.org/10.1029/2012GL051800.

Belt, S.T., 2018. Source-specific biomarkers as proxies for Arctic and Antarctic sea ice. Org. Geochem. 125, 277–298. https://doi.org/10.1016/

j.orggeochem.2018.10.002.
Belt, S.T., Allard, W.G., Massé, G., Robert, J.-M., Rowland, S.J., 2000. Highly branched isoprenoids (HBIs): identification of the most common and abundant sedimentary isomers. Geochem. Cosmochim. Acta 64, 3839–3851. https://doi.org/10.1016/S0016-7037(00)00464-6.
Belt, S.T., Massé, G., Rowland, S.J., Poulin, M., Michel, C., LeBlanc, B., 2007. A novel chemical fossil of palaeo sea ice: IP25. Org. Geochem. 38, 16–27. https://doi.org/10.1016/j.orggeochem.2006.09.013.
Belt, S.T., Cabedo-Sanz, P., Smik, L., Navarro-Rodriguez, A., Berben, S., Knies, J., Husum, K., 2015. Identification of paleo Arctic winter sea ice limits and the marginal ice zone: optimised biomarker-based reconstructions of late Quaternary Arctic sea ice. Earth Planet Sci. Lett. 431, 127–139. https://doi.org/10.1016/j.epsl.2015.09.020.
Belt, S.T., Smik, L., Brown, T., Kim, J.-H., Rowland, S., Allen, C., Gal, J.-K., Shin, K.-H., Lee, J., Taylor, K., 2016. Source identification and distribution reveals the potential of the geochemical Antarctic sea ice proxy IPSO25. Nat. Commun. 7, 12655. https://doi.org/10.1038/ncomms12655.
Belt, S.T., Brown, T.A., Smik, L., Assmy, P., Mundy, C.J., 2018. Sterol identification in floating Arctic sea ice algal aggregates and the Antarctic sea ice diatom Berkeleya adeliensis. Org. Geochem. 118, 1–3. https://doi.org/10.1016/j.orggeochem.2018.01.008.
Berger, A., Loutre, M.F., 1991. Insolation values for the climate of the last 10 million years. Quat. Sci. Rev. 10, 297–317. https://doi.org/10.1016/0277-3791(91)90033-Q.
Birch, L., Cronin, T., Tziperman, E., 2017. Glacial inception on baffin island: the role of insolation, meteorology, and topography. J. Clim. 30, 4047–4064. https://doi.org/10.1175/JCLI-D-16-0576.1.
Boon, J.J., Rijpstra, W.I.C., De Lange, F., De Leeuw, J.W., Yoshioka, M., Shimizu, Y., 1979. Black Sea sterol—a molecular fossil for dinoflagellate blooms. Nature 277, 125–127. https://doi.org/10.1038/277125a0.
Born, A., Stocker, T.F., 2014. Two stable equilibria of the atlantic subpolar gyre. J. Phys. Oceanogr. 44, 246–264. https://doi.org/10.1175/JPO-D-13-073.1.
Born, A., Nisancioglu, K.H., Braconnot, P., 2010. Sea ice induced changes in ocean circulation during the Eemian. Clim. Dynam. 35, 1361–1371. https://doi.org/10.1007/s00382-009-0709-2.
Brown, T.A., Belt, S.T., Tatarek, A., Mundy, C.J., 2014. Source identification of the Arctic sea ice proxy IP25. Nat. Commun. 5, 4197. https://doi.org/10.1038/ncomms5197.
Carlson, A.E., Stoner, J.S., Donnelly, J.P., Hillaire-Marcel, C., 2008. Response of the southern Greenland Ice Sheet during the last two deglaciations. Geology 36, 359–362. https://doi.org/10.1130/G24519A.1.
Channell, J.E.T., Kanamatsu, T., Sato, T., Stein, R., Alvarez Zarikian, C.A., Malone, M.J., and the Expedition 303/306 Scientists, 2006. In: Proceedings of the IODP, 303/306, Proceedings of the IODP. Integrated Ocean Drilling Program. https://doi.org/10.2204/iodp.proc.303306.2006.
Collins, L.G., Allen, C.S., Pike, J., Hodgson, D.A., Weckström, K., Massé, G., 2013. Evaluating highly branched isoprenoid (HBI) biomarkers as a novel Antarctic sea-ice proxy in deep ocean glacial age sediments. Quat. Sci. Rev. 79, 87–98. https://doi.org/10.1016/j.quascirev.2013.02.004.
Colville, E.J., Carlson, A.E., Beard, B.L., Hatfield, R.G., Stoner, J.S., Reyes, A.V., Ullman, D.J., 2011. Sr-Nd-Pb isotope evidence for ice-sheet presence on southern Greenland during the last interglacial. Science 333, 620–623. https://doi.org/10.1126/science.1204673.
Condron, A., Winsor, P., 2012. Meltwater routing and the younger Dryas. Proc. Natl. Acad. Sci. USA 109, 19928–19933. https://doi.org/10.1073/pnas.1207381109.
Cortese, G., Dolven, J.K., Bjørklund, K.R., Malmgren, B.A., 2005. Late Pleistocene–Holocene radiolarian paleotemperatures in the Norwegian Sea based on artificial neural networks. Palaeogeogr. Palaeoclimatol. Palaeoecol. 224, 311–332. https://doi.org/10.1016/j.palaeo.2005.04.015.
Dale, B., 1996. Chapter 31. Dinoflagellate cyst ecology: modeling and geological applications. In: Jansonius, J., McGregor, D.C. (Eds.), Palynology: Principles and Applications, vol. 3. American Association of Stratigraphic Palynologists Foundation, Dallas, TX, pp. 1249–1275.
Dale, B., 2001. The sedimentary record of dinoflagellate cysts: looking back into the future of phytoplankton blooms. Sci. Mar. 65, 257–272. https://doi.org/10.3989/scimar.2001.65s2257.
Dalton, A.S., Stokes, C.R., Batchelor, C.L., 2022. Evolution of the Laurentide and innuitian ice sheets prior to the last glacial maximum (115 ka to 25 ka). Earth Sci. Rev. 224, 103875. https://doi.org/10.1016/j.earscirev.2021.103875.
de Schepper, S., Beck, K.M., Mangerud, G., 2017. Late neogene dinoflagellate cyst and acritarch biostratigraphy for Ocean Drilling program hole 642B, Norwegian sea. Rev. Palaeobot. Palynol. https://doi.org/10.1016/j.revpalbo.2016.08.005.
de Vernal, A., Hillaire-Marcel, C., 2008. Natural variability of Greenland climate, vegetation, and ice volume during the past million years. Science 320, 1622–1625. https://doi:10.1126/science.1153929.
de Vernal, A., Marret, F., 2007. Organic-walled dinoflagellate cysts: tracers of sea-surface conditions. In: Hillaire-Marcel, C., de Vernal, A. (Eds.), Proxies in Late Cenozoic Paleoceanography, vol. 1. Elsevier, Rotterdam, pp. 371–408. https://doi.org/10.1016/S1572-5480(07)01014-7.
de Vernal, A., Rochon, A., Turon, J.-L., Matthiessen, J., 1997. Organic-walled dinoflagellate cysts: palynological tracers of sea-surface conditions in middle to high latitude marine environments. Geobios 30, 905–920. https://doi.org/10.1016/S0016-6995(97)80215-X.
de Vernal, A., Hillaire-Marcel, C., Turon, J.-L., Matthiessen, J., 2000. Reconstruction of sea-surface temperature, salinity, and sea-ice cover in the northern North Atlantic during the last glacial maximum based on dinocyst assemblages. Can. J. Earth Sci. 37, 725–750. https://doi.org/10.1139/e99-091.
de Vernal, A., Eynaud, F., Henry, M., Hillaire-Marcel, C., Londeix, L., Mangin, S., Matthiessen, J., Marret, F., Radi, T., Rochon, A., Solignac, S., Turon, J.-L., 2005. Reconstruction of sea-surface conditions at middle to high latitudes of the Northern Hemisphere during the Last Glacial Maximum (LGM) based on dinoflagellate cyst assemblages. Quat. Sci. Rev. 24, 897–924. https://doi.org/10.1016/j.quascirev.2004.06.014.
de Vernal, A., Gersonde, R., Goosse, H., Seidenkrantz, M.-S., Wolff, E.W., 2013. Sea ice in the paleoclimate system: the challenge of reconstructing sea ice from proxies – an introduction. Quat. Sci. Rev. 79, 1–8. https://doi.org/10.1016/j.quascirev.2013.08.009.
de Vernal, A., Radi, T., Zaragosi, S., Van Nieuwenhove, N., Rochon, A., Allan, E., De Schepper, S., Eynaud, F., Head, M.J., Limoges, A., Londeix, L., Marret, F., Matthiessen, J., Penaud, A., Pospelova, V., Price, A., Richerol, T., 2020. Distribution of common modern dinoflagellate cyst taxa in surface sediments of the Northern Hemisphere in relation to environmental parameters: the new n=1968 database. Mar. Micropaleontol. 159, 101796. https://doi.org/10.1016/j.marmicro.2019.101796.
Dokken, T.M., Nisancioglu, K.H., Li, C., Battisti, D.S., Kissel, C., 2013. Dansgaard-Oeschger cycles: interactions between ocean and sea ice intrinsic to the Nordic seas. Paleoceanography 28, 491–502. https://doi.org/10.1002/palo.20042.
Eynaud, F., Turon, J.L., Duprat, J., 2004. Comparison of the Holocene and eemian palaeoenvironments in the South Icelandic basin: dinoflagellate cysts as proxies for the North atlantic surface circulation. Rev. Palaeobot. Palynol. 128, 55–79. https://doi.org/10.1016/S0034-6667(03)00112-X.
Fahl, K., Stein, R., 2012. Modern seasonal variability and deglacial/Holocene change of central Arctic Ocean sea-ice cover: new insights from biomarker proxy records. Earth Planet Sci. Lett. 351 (352), 123–133. https://doi.org/10.1016/j.epsl.2012.07.009.
Foukal, N.P., Lozier, M.S., 2017. Assessing variability in the size and strength of the North Atlantic subpolar gyre. J. Geophys. Res. 122, 6295–6308. https://doi.org/10.1002/2017JC012798.
Galaasen, E.V., Ninnemann, U.S., Irvali, N., Kleiven, H.F., Rosenthal, Y., Kissel, C., Hodell, D.A., 2014. Rapid reductions in North Atlantic deep water during the peak of the last Interglacial period. Science 343, 1129–1132. https://doi.org/10.1126/science.1248667.
Griem, L., Voelker, A.H.L., Berben, S.M.P., Dokken, T.M., Jansen, E., 2019. Insolation and glacial meltwater influence on sea-ice and circulation variability in the northeastern Labrador Sea during the last glacial period. Paleoceanogr. Paleoclimatol. 34, 1689–1709. https://doi.org/10.1029/2019PA003605.
Grøsfjeld, K., Funder, S., Seidenkrantz, M.-S., Glaister, C., 2006. Last Interglacial marine environments in the White Sea region, northwestern Russia. Boreas 35, 493–520. https://doi.org/10.1080/03009480600781917.
Grøsfjeld, K., Harland, R., Howe, J., 2009. Dinoflagellate cyst assemblages inshore and offshore Svalbard reflecting their modern hydrography and climate. Norw. J. Geol. 89, 129–134.
Häkkinen, S., Rhines, P.B., 2004. Decline of subpolar North Atlantic circulation during the 1990s. Science 304, 555–559.
Hátún, H., Sandø, A.B., Drange, H., Hansen, B., Valdimarsson, H., 2005. Influence of the atlantic subpolar gyre on the thermohaline circulation. Science 309, 1841–1844.
Head, M.J., Lewis, J., de Vernal, A., 2006. The cyst of the calcareous dinoflagellate Scrippsiella trifida: resolving the fossil record of its organic wall with that of Alexandrium tamarense. J. Paleontol. 80, 1–18. https://doi.org/10.1666/0022-3360(2006)080[0001:TCOTCD]2.0.CO;2.
Hennissen, J.A.I., Head, M.J., de Schepper, S., Groeneveld, J., 2014. Palynological evidence for a southward shift of the North atlantic current at 2.6 ma during the intensification of late cenozoic northern hemisphere glaciation. Paleoceanography 29, 564–580. https://doi.org/10.1002/2013PA002543.
Hennissen, J.A.I., Head, M.J., de Schepper, S., Groeneveld, J., 2017. Dinoflagellate cyst paleoecology during the pliocene–pleistocene climatic transition in the North atlantic. Palaeogeogr. Palaeoclimatol. Palaeoecol. 470, 81–108. https://doi.org/10.1016/j.palaeo.2016.12.023.
Heslop, D., de Schepper, S., Proske, U., 2011. Diagnosing the uncertainty of taxa relative abundances derived from count data. Mar. Micropaleontol. 79, 114–120. https://doi.org/10.1016/j.marmicro.2011.01.007.
Hillaire-Marcel, de Vernal, A., Bilodeau, G., Wu, G., 1994. Isotope stratigraphy, sedimentation rates, deep circulation, and carbonate events in the Labrador Sea during the last ~200ka. Can. J. Earth Sci. 31, 63–89. https://doi.org/10.1139/e94-007.
Hillaire-Marcel, C., de Vernal, A., Bilodeau, G., Weaver, A., 2001. Absence of deep-water formation in the Labrador Sea during the last Interglacial period. Nature 410, 1073–1077. https://doi.org/10.1038/35074059.
Hillaire-Marcel, C., de Vernal, A., Piper, D.J.W., 2007. Lake Agassiz final drainage event in the northwest North Atlantic. Geophys. Res. Lett. 34. https://doi.org/10.1029/2007GL030396.
Hodell, D.A., Minth, E.K., Curtis, J.H., McCave, I.N., Hall, I.R., Channell, J.E.T., Xuan, C., 2009. Surface and deep-water hydrography on Gardar Drift (Iceland Basin) during the last interglacial period. Earth Planet Sci. Lett. 288, 10–19. https://doi.org/10.1016/j.epsl.2009.08.040.
Hu, A., Meehl, G.A., Otto-Bliesner, B.L., Waelbroeck, C., Han, W., Loutre, M.-F., Lambeck, K., Mitrovica, J.X., Rosenbloom, N., 2010. Influence of Bering Strait flow and North Atlantic circulation on glacial sea-level changes. Nat. Geosci. 3, 118–121. https://doi.org/10.1038/ngeo729.

Huang, W.-Y., Meinschein, W.G., 1979. Sterols as ecological indicators. Geochem. Cosmochim. Acta 43, 739–745. https://doi.org/10.1016/0016-7037(79)90257-6.
Hunter, S., Wilkinson, D., Louarn, E., Nick McCave, I., Rohling, E., Stow, D.A.V., Bacon, S., 2007. Deep western boundary current dynamics and associated sedimentation on the Eirik Drift, Southern Greenland Margin. Deep Sea Res. Oceanogr. Res. Pap. 54, 2036–2066. https://doi.org/10.1016/j.dsr.2007.09.007.
Irvali, N., Ninnemann, U.S., Galaasen, E.V., Rosenthal, Y., Kroon, D., Oppo, D.W., Kleiven, H.F., Darling, K.F., Kissel, C., 2012. Rapid switches in subpolar North Atlantic hydrography and climate during the Last Interglacial (MIS 5e). Paleoceanography 27. https://doi.org/10.1029/2011PA002244.
Irvali, N., Ninnemann, U.S., Kleiven, H.F., Galaasen, E.V., Morley, A., Rosenthal, Y., 2016. Evidence for regional cooling, frontal advances, and East Greenland Ice Sheet changes during the demise of the last interglacial. Quat. Sci. Rev. 150, 184–199. https://doi.org/10.1016/j.quascirev.2016.08.029.
Jaffé, R., Wolff, G.A., Cabrera, A.C., Chitty, H.C., 1995. The biogeochemistry of lipids in rivers of the Orinoco Basin. Geochem. Cosmochim. Acta 59, 4507–4522. https://doi.org/10.1016/0016-7037(95)00246-V.
Johns, L., Wraige, E.J., Belt, S.T., Lewis, C.A., Massé, G., Robert, J.-M., Rowland, S.J., 1999. Identification of a C25 highly branched isoprenoid (HBI) diene in Antarctic sediments, Antarctic sea-ice diatoms and cultured diatoms. Org. Geochem. 30, 1471–1475. https://doi.org/10.1016/S0146-6380(99)00112-6.
Jonkers, L., Brummer, G.-J.A., Peeters, F.J.C., van Aken, H.M., De Jong, M.F., 2010. Seasonal stratification, shell flux, and oxygen isotope dynamics of left-coiling N. pachyderma and T. quinqueloba in the western subpolar North Atlantic. Paleoceanography 25. https://doi.org/10.1029/2009PA001849.
Kageyama, M., Sime, L.C., Sicard, M., Guarino, M.-V., de Vernal, A., Stein, R., Schroeder, D., Malmierca-Vallet, I., Abe-Ouchi, A., Bitz, C., Braconnot, P., Brady, E.C., Cao, J., Chamberlain, M.A., Feltham, D., Guo, C., LeGrande, A.N., Lohmann, G., Meissner, K.J., Menviel, L., Morozova, P., Nisancioglu, K.H., Otto-Bliesner, B.L., O'ishi, R., Ramos Buarque, S., Salas y Melia, D., Sherriff-Tadano, S., Stroeve, J., Shi, X., Sun, B., Tomas, R.A., Volodin, E., Yeung, N.K.H., Zhang, Q., Zhang, Z., Zheng, W., Ziehn, T., 2021. A multi-model CMIP6-PMIP4 study of Arctic sea ice at 127: sea ice data compilation and model differences. Clim. Past 17, 37–62. https://doi.org/10.5194/cp-17-37-2021.
Karami, M.P., Myers, P.G., de Vernal, A., Tremblay, L.B., Hu, X., 2021. The role of Arctic gateways on sea ice and circulation in the Arctic and North Atlantic Oceans: a sensitivity study with an ocean-sea-ice model. Clim. Dynam. 57, 2129–2151. https://doi.org/10.1007/s00382-021-05798-6.
Kerwin, M.W., 1996. A regional stratigraphic isochron (ca. 800014C yr B.P.) from final deglaciation of Hudson Strait. Quat. Res. 46, 89–98. https://doi.org/10.1006/qres.1996.0049.
Kessler, A., Bouttes, N., Roche, D.M., Ninnemann, U.S., Galaasen, E.V., Tjiputra, J., 2020. Atlantic meridional overturning circulation and δ13C variability during the last interglacial. Paleoceanogr. Paleoclimatol. 35, e2019PA003818. https://doi.org/10.1029/2019PA003818.
Kleman, J., Jansson, K., De Angelis, H., Stroeven, A.P., Hättestrand, C., Alm, G., Glasser, N., 2010. North American Ice Sheet build-up during the last glacial cycle, 115–21kyr. Quat. Sci. Rev. 29, 2036–2051. https://doi.org/10.1016/j.quascirev.2010.04.021.
Klockmann, M., Mikolajewicz, U., Kleppin, H., Marotzke, J., 2020. Coupling of the subpolar gyre and the overturning circulation during abrupt glacial climate transitions. Geophys. Res. Lett. 47, e2020GL090361. https://doi.org/10.1029/2020GL090361.
Kolling, H.M., Stein, R., Fahl, K., Sadatzki, H., de Vernal, A., Xiao, X., 2020. Biomarker distributions in (Sub)-Arctic surface sediments and their potential for Sea Ice reconstructions. G-cubed 21, e2019GC008629. https://doi.org/10.1029/2019GC008629.
Kopp, R.E., Simons, F.J., Mitrovica, J.X., Maloof, A.C., Oppenheimer, M., 2009. Probabilistic assessment of sea level during the last interglacial stage. Nature 462, 863–867. https://doi.org/10.1038/nature08686.
Kozdon, R., Eisenhauer, A., Weinelt, M., Meland, M.Y., Nürnberg, D., 2009. Reassessing Mg/Ca temperature calibrations of Neogloboquadrina pachyderma (sinistral) using paired δ44/40Ca and Mg/Ca measurements. G-cubed 10, Q03005. https://doi.org/10.1029/2008GC002169.
Kremer, A., Stein, R., Fahl, K., Bauch, H., Mackensen, A., Niessen, F., 2018a. A 190-ka biomarker record revealing interactions between sea ice, Atlantic Water inflow and ice sheet activity in eastern Fram Strait. Arktos 4, 22. https://doi.org/10.1007/s41063-018-0052-0.
Kremer, A., Stein, R., Fahl, K., Ji, Z., Yang, Z., Wiers, S., Matthiessen, J., Forwick, M., Löwemark, L., O'Regan, M., Chen, J., Snowball, I., 2018b. Changes in sea ice cover and ice sheet extent at the Yermak Plateau during the last 160 ka – reconstructions from biomarker records. Quat. Sci. Rev. 182, 93–108. https://doi.org/10.1016/j.quascirev.2017.12.016.
Lajeunesse, P., St-Onge, G., 2008. The subglacial origin of the Lake Agassiz–Ojibway final outburst flood. Nat. Geosci. 1, 184–188. https://doi.org/10.1038/ngeo130.
Lambeck, K., Chappell, J., 2001. Sea level change through the last glacial cycle. Science 292, 679–686. https://doi.org/10.1126/science.1059549.
Leduc, G., Schneider, R., Kim, J.-H., Lohmann, G., 2010. Holocene and Eemian sea surface temperature trends as revealed by alkenone and Mg/Ca paleothermometry. Quat. Sci. Rev. 29, 989–1004. https://doi.org/10.1016/j.quascirev.2010.01.004.
Levermann, A., Born, A., 2007. Bistability of the Atlantic subpolar gyre in a coarse-resolution climate model. Geophys. Res. Lett. 34. https://doi.org/10.1029/2007GL031732.
Li, C., Born, A., 2019. Coupled atmosphere-ice-ocean dynamics in Dansgaard-Oeschger events. Quat. Sci. Rev. 203, 1–20. https://doi.org/10.1016/j.quascirev.2018.10.031.
Limoges, A., Ribeiro, S., Weckström, K., Heikkilä, M., Zamelczyk, K., Andersen, T.J., Seidenkrantz, M.S., 2018. Linking the modern distribution of biogenic proxies in high Arctic Greenland shelf sediments to sea ice, primary production, and Arctic-Atlantic inflow. J. Geophys. Res.: Biogeosciences 123, 760–786. https://doi.org/10.1002/2017JG003840.
Locarnini, R.A., Mishonov, A.V., Baranova, O.K., Boyer, T.P., Zweng, M.M., Garcia, H.E., Reagan, J.R., Seidov, D., Weathers, K., Paver, C.R., Smolyar, I., 2019. In: Mishonov Technical, A. (Ed.), World Ocean Atlas 2018, Volume 1: Temperature, NOAA Atlas NESDIS, vol. 81, p. 52pp.
Lofverstrom, M., Thompson, D.M., Otto-Bliesner, B.L., Brady, E.C., 2022. The importance of Canadian Arctic Archipelago gateways for glacial expansion in Scandinavia. Nat. Geosci. 15, 482–488. https://doi.org/10.1038/s41561-022-00956-9.
Lohmann, K., Drange, H., Bentsen, M., 2009. Response of the North Atlantic subpolar gyre to persistent North Atlantic oscillation like forcing. Clim. Dynam. 32, 273–285. https://doi.org/10.1007/s00382-008-0467-6.
Lozier, M.S., 2012. Overturning in the North atlantic. Ann. Rev. Mar. Sci 4, 291–315. https://doi.org/10.1146/annurev-marine-120710-100740.
Lozier, M.S., Li, F., Bacon, S., Bahr, F., Bower, A.S., Cunningham, S.A., de Jong, M.F., de Steur, L., deYoung, B., Fischer, J., Gary, S.F., Greenan, B.J.W., Holliday, N.P., Houk, A., Houpert, L., Inall, M.E., Johns, W.E., Johnson, H.L., Johnson, C., Karstensen, J., Koman, G., Le Bras, I.A., Lin, X., Mackay, N., Marshall, D.P., Mercier, H., Oltmanns, M., Pickart, R.S., Ramsey, A.L., Rayner, D., Straneo, F., Thierry, V., Torres, D.J., Williams, R.G., Wilson, C., Yang, J., Yashayaev, I., Zhao, J., 2019. A sea change in our view of overturning in the subpolar North Atlantic. Science 363, 516–521. https://doi.org/10.1126/science.aau6592.
Lüthi, D., Le Floch, M., Bereiter, B., Blunier, T., Barnola, J.-M., Siegenthaler, U., Raynaud, D., Jouzel, J., Fischer, H., Kawamura, K., Stocker, T.F., 2008. High-resolution carbon dioxide concentration record 650,000–800,000 years before present. Nature 453, 379–382. https://doi.org/10.1038/nature06949.
Marret, F., Zonneveld, K.A.F., 2003. Atlas of modern organic-walled dinoflagellate cyst distribution. Rev. Palaeobot. Palynol. 125, 1–200. https://doi.org/10.1016/S0034-6667(02)00229-4.
Marret, F., Eiríksson, J., Knudsen, K.L., Turon, J.-L., Scourse, J.D., 2004. Distribution of dinoflagellate cyst assemblages in surface sediments from the northern and western shelf of Iceland. Rev. Palaeobot. Palynol. 128, 35–53. https://doi.org/10.1016/S0034-6667(03)00111-8.
Matthiessen, J., Knies, J., 2001. Dinoflagellate cyst evidence for warm interglacial conditions at the northern Barents Sea margin during marine oxygen isotope stage 5. J. Quat. Sci. 16, 727–737. https://doi.org/10.1002/jqs.656.
Matthiessen, J., Knies, J., Nowaczyk, N.R., Stein, R., 2001. Late Quaternary dinoflagellate cyst stratigraphy at the Eurasian continental margin, Arctic Ocean: indications for Atlantic water inflow in the past 150,000 years. Global Planet. Change 31, 65–86. https://doi.org/10.1016/S0921-8181(01)00113-8.
Max, L., Nürnberg, D., Chiessi, C.M., Lenz, M.M., Mulitza, S., 2022. Subsurface ocean warming preceded Heinrich Events. Nat. Commun. 13, 4217. https://doi.org/10.1038/s41467-022-31754-x.
Mengel, M., Levermann, A., Schleussner, C.-F., Born, A., 2012. Enhanced Atlantic subpolar gyre variability through baroclinic threshold in a coarse resolution model. Earth System Dynamics 3, 189–197. https://doi.org/10.5194/esd-3-189-2012.
Mokeddem, Z., McManus, J.F., 2016. Persistent climatic and oceanographic oscillations in the subpolar North Atlantic during the MIS 6 glaciation and MIS 5 interglacial. Paleoceanography 31, 758–778. https://doi.org/10.1002/2015PA002813.
Mokeddem, Z., McManus, J.F., Oppo, D.W., 2014. Oceanographic dynamics and the end of the last interglacial in the subpolar North Atlantic. Proc. Natl. Acad. Sci. USA 111, 11263–11268. https://doi.org/10.1073/pnas.1322103111.
Montoya, M., Born, A., Levermann, A., 2011. Reversed North Atlantic gyre dynamics in present and glacial climates. Clim. Dynam. 36, 1107–1118. https://doi.org/10.1007/s00382-009-0729-y.
Müller, J., Massé, G., Stein, R., Belt, S.T., 2009. Variability of sea-ice conditions in the Fram Strait over the past 30,000 years. Nat. Geosci. 2, 772–776. https://doi.org/10.1038/ngeo665.
Müller, J., Wagner, A., Fahl, K., Stein, R., Prange, M., Lohmann, G., 2011. Towards quantitative sea ice reconstructions in the northern North Atlantic: a combined biomarker and numerical modelling approach. Earth Planet Sci. Lett. 306, 137–148. https://doi.org/10.1016/j.epsl.2011.04.011.
Münchow, A., Falkner, K.K., Melling, H., 2015. Baffin island and west Greenland current systems in northern baffin bay. Prog. Oceanogr. 132, 305–317. https://doi.org/10.1016/j.pocean.2014.04.001.
Nicholl, J.A.L., Hodell, D.A., Naafs, B.D.A., Hillaire-Marcel, C., Channell, J.E.T., Romero, O.E., 2012. A Laurentide outburst flooding event during the last interglacial period. Nat. Geosci. 5, 901–904. https://doi.org/10.1038/ngeo1622.
Oppo, D.W., McManus, J.F., Cullen, J.L., 2006. Evolution and demise of the last interglacial warmth in the subpolar North Atlantic. Quat. Sci. Rev. 25, 3268–3277. https://doi.org/10.1016/j.quascirev.2006.07.006.
Otto-Bliesner, B.L., Marshall, S.J., Overpeck, J.T., Miller, G.H., Hu, A., Members of CAPE Last Interglacial Project, 2006. Simulating arctic climate warmth and icefield retreat in the last interglaciation. Science 311, 1751–1753.
Pados, T., Spielhagen, R.F., 2014. Species distribution and depth habitat of recent planktic foraminifera in Fram Strait, Arctic Ocean. Polar Res. 33, 22483. https://doi.org/10.3402/polar.v33.22483.
Paillard, D., Labeyrie, L., Yiou, P., 1996. Macintosh Program performs time-series

analysis. Eos, Transactions American Geophysical Union 77, 379. https://doi.org/10.1029/96EO00259, 379.
Penaud, A., Eynaud, F., Turon, J.L., Zaragosi, S., Marret, F., Bourillet, J.F., 2008. Interglacial variability (MIS 5 and MIS 7) and dinoflagellate cyst assemblages in the bay of biscay (North Atlantic). Mar. Micropaleontol. 68, 136–155. https://doi.org/10.1016/j.marmicro.2008.01.007.
Prinsenberg, S.J., Hamilton, J., 2005. Monitoring the volume, freshwater and heat fluxes passing through Lancaster sound in the Canadian arctic archipelago. Atmos.-Ocean 43, 1–22. https://doi.org/10.3137/ao.430101.
Pryce, R.J., 1971. The occurrence of bound, water-soluble squalene, 4,4-dimethyl sterols, 4α-methyl sterols and sterols in leaves of Kalanchoe blossfeldiana. Phytochemistry 10, 1303–1307. https://doi.org/10.1016/S0031-9422(00)84332-0.
Radi, T., Vernal, A. de, Peyron, O., 2001. Relationships between dinoflagellate cyst assemblages in surface sediment and hydrographic conditions in the Bering and Chukchi seas. J. Quat. Sci. 16, 667–680. https://doi.org/10.1002/jqs.652.
Risebrobakken, B., Balbon, E., Dokken, T., Jansen, E., Kissel, C., Labeyrie, L., Richter, T., Senneset, L., 2006. The penultimate deglaciation: high-resolution paleoceanographic evidence from a north–south transect along the eastern Nordic Seas. Earth Planet Sci. Lett. 241, 505–516. https://doi.org/10.1016/j.epsl.2005.11.032.
Risebrobakken, B., Dokken, T., Otterå, O.H., Jansen, E., Gao, Y., Drange, H., 2007. Inception of the Northern European ice sheet due to contrasting ocean and insolation forcing. Quat. Res. 67, 128–135. https://doi.org/10.1016/j.yqres.2006.07.007.
Risebrobakken, B., Dokken, T., Smedsrud, L.H., Andersson, C., Jansen, E., Moros, M., Ivanova, E.V., 2011. Early Holocene temperature variability in the Nordic Seas: the role of oceanic heat advection versus changes in orbital forcing. Paleoceanography 26. https://doi.org/10.1029/2011PA002117.
Robinson, N., Eglinton, G., Brassell, S.C., Cranwell, P.A., 1984. Dinoflagellate origin for sedimentary 4α-methylsteroids and 5α(H)-stanols. Nature 308, 439–442. https://doi.org/10.1038/308439a0.
Rochon, A., de Vernal, A., Turon, J.-L., Matthiessen, J., Head, M.J., 1999. Distribution of recent dinoflagellate cysts in surface sediments from the North Atlantic Ocean and adjacent seas in relation to sea-surface parameters. Am. Assoc. Stratigr. Palynol. Contrib. Ser. 35, 1–146.
Rohling, E.J., Hibbert, F.D., Grant, K.M., Galaasen, E.V., Irvalı, N., Kleiven, H.F., Marino, G., Ninnemann, U., Roberts, A.P., Rosenthal, Y., Schulz, H., Williams, F.H., Yu, J., 2019. Asynchronous Antarctic and Greenland ice-volume contributions to the last interglacial sea-level highstand. Nat. Commun. 10, 5040. https://doi.org/10.1038/s41467-019-12874-3.
Rontani, J.-F., Charrière, B., Sempéré, R., Doxaran, D., Vaultier, F., Vonk, J.E., Volkman, J.K., 2014. Degradation of sterols and terrigenous organic matter in waters of the Mackenzie Shelf, Canadian Arctic. Org. Geochem. 75, 61–73. https://doi.org/10.1016/j.orggeochem.2014.06.002.
Rudels, B., Korhonen, M., Schauer, U., Pisarev, S., Rabe, B., Wisotzki, A., 2015. Circulation and transformation of atlantic water in the eurasian basin and the contribution of the Fram Strait inflow branch to the Arctic Ocean heat budget. Prog. Oceanogr. 132, 128–152. https://doi.org/10.1016/j.pocean.2014.04.003.
Sánchez Goñi, M.F., Eynaud, F., Turon, J.L., Shackleton, N.J., 1999. High resolution palynological record off the Iberian margin: direct land-sea correlation for the Last Interglacial complex. Earth Planet Sci. Lett. 171, 123–137. https://doi.org/10.1016/S0012-821X(99)00141-7.
Sánchez Goñi, M.F., Loutre, M.F., Crucifix, M., Peyron, O., Santos, L., Duprat, J., Malaizé, B., Turon, J.-L., Peypouquet, J.-P., 2005. Increasing vegetation and climate gradient in Western Europe over the Last Glacial Inception (122–110 ka): data-model comparison. Earth Planet Sci. Lett. 231, 111–130. https://doi.org/10.1016/j.epsl.2004.12.010.
Sarnthein, M., Tiedemann, R., 1990. Younger dryas-style cooling events at glacial terminations I-vi at ODP site 658: associated benthic δ13C anomalies constrain meltwater hypothesis. Paleoceanography 5, 1041–1055. https://doi.org/10.1029/PA005i006p01041.
Scoto, F., Sadatzki, H., Maffezzoli, N., Barbante, C., Gagliardi, A., Varin, C., Vallelonga, P., Gkinis, V., Dahl-Jensen, D., Kjaer, H.A., Burgay, F., Saiz-Lopez, A., Stein, R., Spolaor, A., 2022. Sea ice fluctuations in the Baffin Bay and the Labrador Sea during glacial abrupt climate changes. Proc. Natl. Acad. Sci. USA 119, e2203468119. https://doi.org/10.1073/pnas.2203468119.
Seidenkrantz, M.-S., Kristensen, P., Knudsen, K.L., 1995. Marine evidence for climatic instability during the last interglacial in shelf records from northwest Europe. J. Quat. Sci. 10, 77–82. https://doi.org/10.1002/jqs.3390100108.
Seidenkrantz, M.-S., Bornmalm, L., Johnsen, S.J., Knudsen, K.L., Kuijpers, A., Lauritzen, S.-E., Leroy, S.A.G., Mergeal, I., Schweger, C., Van Vliet-Lanoë, B., 1996. Two-step deglaciation at the oxygen isotope stage 6/5E transition: the Zeifen-Kattegat climate oscillation. Quat. Sci. Rev. 15, 63–75. https://doi.org/10.1016/0277-3791(95)00086-0.
Shackleton, N., Chapman, M., Sanchez Goñi, M., Pailler, D., Lancelot, Y., 2002. The Classic Marine Isotope Substage 5e. Quat. Res. 58, 14–16. https://doi.org/10.1006/qres.2001.2312.
Shackleton, N.J., Sánchez-Goñi, M.F., Pailler, D., Lancelot, Y., 2003. Marine Isotope Substage 5e and the Eemian Interglacial. Global Planet. Change 36, 151–155. https://doi.org/10.1016/S0921-8181(02)00181-9.
Shaw, J., Lesemann, J.-E., 2003. Subglacial outburst floods and extreme sedimentary events in the Labrador Sea. In: Chan, M.A., Archer, A.W. (Eds.), Extreme Depositional Environments: Mega End Members in Geologic Time. Geological Society of America. https://doi.org/10.1130/0-8137-2370-1.25, 0.
Simstich, J., Sarnthein, M., Erlenkeuser, H., 2003. Paired δ18O signals of Neogloboquadrina pachyderma (s) and Turborotalita quinqueloba show thermal stratification structure in Nordic Seas. Mar. Micropaleontol. 48, 107–125. https://doi.org/10.1016/S0377-8398(02)00165-2.
Smedsrud, L.H., Muilwijk, M., Brakstad, A., Madonna, E., Lauvset, S.K., Spensberger, C., Born, A., Eldevik, T., Drange, H., Jeansson, E., Li, C., Olsen, A., Skagseth, Ø., Slater, D.A., Straneo, F., Våge, K., Årthun, M., 2022. Nordic seas heat loss, atlantic inflow, and arctic Sea Ice cover over the last century. Rev. Geophys. 60, e2020RG000725. https://doi.org/10.1029/2020RG000725.
Solignac, S., Grøsfjeld, K., Giraudeau, J., de Vernal, A., 2009. Distribution of recent dinocyst assemblages in the western Barents Sea. Norw. J. Geol. 11.
Spratt, R., Lisiecki, L., 2016. A Late Pleistocene sea level stack. Clim. Past 12, 1079–1092. https://doi.org/10.5194/cpd-11-3699-2015.
St-Onge, G., Lajeunesse, P., 2007. Flood-Induced turbidites from northern Hudson bay and western Hudson Strait: a two-pulse record of lake Agassiz final outburst flood?. In: Lykousis, V., Sakellariou, D., Locat, J. (Eds.), Submarine Mass Movements and Their Consequences. Advances in Natural and Technological Hazards Research, vol. 27. Springer, Dordrecht. https://doi.org/10.1007/978-1-4020-6512-5_14.
Stein, R., Fahl, K., Gierz, P., Niessen, F., Lohmann, G., 2017. Arctic Ocean sea ice cover during the penultimate glacial and the last interglacial. Nat. Commun. 8, 1–13. https://doi.org/10.1038/s41467-017-00552-1.
Stein, R., Kremer, A., Fahl, K., 2022. Past glacial-interglacial changes in Arctic Ocean sea-ice conditions. Past Global Changes Magazine 30, 90–91. https://doi.org/10.22498/pages.30.2.90.
Stirling, C.H., Esat, T.M., Lambeck, K., McCulloch, M.T., 1998. Timing and duration of the Last Interglacial: evidence for a restricted interval of widespread coral reef growth. Earth Planet Sci. Lett. 160, 745–762. https://doi.org/10.1016/S0012-821X(98)00125-3.
Stockmarr, J., 1971. Tablets with spores used in absolute pollen analysis. Pollen Spores 13, 615–621.
Stokes, C.R., Tarasov, L., Dyke, A.S., 2012. Dynamics of the North American ice sheet complex during its inception and build-up to the last glacial maximum. Quat. Sci. Rev. 50, 86–104. https://doi.org/10.1016/j.quascirev.2012.07.009.
Svendsen, J.I., Alexanderson, H., Astakhov, V.I., Demidov, I., Dowdeswell, J.A., Funder, S., Gataullin, V., Henriksen, M., Hjort, C., Houmark-Nielsen, M., Hubberten, H.W., Ingólfsson, Ó., Jakobsson, M., Kjær, K.H., Larsen, E., Lokrantz, H., Lunkka, J.P., Lyså, A., Mangerud, J., Matiouchkov, A., Murray, A., Möller, P., Niessen, F., Nikolskaya, O., Polyak, L., Saarnisto, M., Siegert, C., Siegert, M.J., Spielhagen, R.F., Stein, R., 2004. Late Quaternary ice sheet history of northern Eurasia. Quat. Sci. Rev. 23, 1229–1271. https://doi.org/10.1016/j.quascirev.2003.12.008.
Thornalley, D.J.R., Elderfield, H., McCave, I.N., 2009. Holocene oscillations in temperature and salinity of the surface subpolar North Atlantic. Nature 457, 711–714. https://doi.org/10.1038/nature07717.
Tzedakis, P.C., Drysdale, R.N., Margari, V., Skinner, L.C., Menviel, L., Rhodes, R.H., Taschetto, A.S., Hodell, D.A., Crowhurst, S.J., Hellstrom, J.C., Fallick, A.E., Grimalt, J.O., McManus, J.F., Martrat, B., Mokeddem, Z., Parrenin, F., Regattieri, E., Roe, K., Zanchetta, G., 2018. Enhanced climate instability in the North atlantic and southern europe during the last interglacial. Nat. Commun. 9, 4235. https://doi.org/10.1038/s41467-018-06683-3.
Van Nieuwenhove, N., Bauch, H.A., Matthiessen, J., 2008. Last interglacial surface water conditions in the eastern Nordic Seas inferred from dinocyst and foraminiferal assemblages. Mar. Micropaleontol. 66, 247–263. https://doi.org/10.1016/j.marmicro.2007.10.004.
Van Nieuwenhove, N., Bauch, H.A., Eynaud, F., Kandiano, E., Cortijo, E., Turon, J.-L., 2011. Evidence for delayed poleward expansion of North Atlantic surface waters during the last interglacial (MIS 5e). Quat. Sci. Rev. 30, 934–946. https://doi.org/10.1016/j.quascirev.2011.01.013.
Van Nieuwenhove, N., Baumann, A., Matthiessen, J., Bonnet, S., de Vernal, A., 2016. Sea surface conditions in the southern Nordic Seas during the Holocene based on dinoflagellate cyst assemblages. Holocene 26, 722–735. https://doi.org/10.1177/0959683615618258.
Van Nieuwenhove, N., Pearce, C., Knudsen, M.F., Røy, H., Seidenkrantz, M.-S., 2018. Meltwater and seasonality influence on subpolar gyre circulation during the Holocene. Palaeogeogeography, Palaeoclimatology, Palaeoecology. 502, 104–118. https://doi.org/10.1016/j.palaeo.2018.05.002.
Vettoretti, G., Peltier, W., 2003. Post-eemian glacial inception. Part I: the impact of summer seasonal temperature bias. J. Clim. 16, 889–911. https://doi.org/10.1175/1520-0442(2003)016<0889:PEGIPI>2.0.CO;2.
Volkman, J.K., 1986. A review of sterol markers for marine and terrigenous organic matter. Org. Geochem. 9, 83–99. https://doi.org/10.1016/0146-6380(86)90089-6.
Volkman, J.K., Barrett, S.M., Blackburn, S.I., Mansour, M.P., Sikes, E.L., Gelin, F., 1998. Microalgal biomarkers: a review of recent research developments. Org. Geochem. 29, 1163–1179. https://doi.org/10.1016/S0146-6380(98)00062-X.
Waelbroeck, C., Labeyrie, L., Michel, E., Duplessy, J.C., McManus, J.F., Lambeck, K., Balbon, E., Labracherie, M., 2002. Sea-level and deep water temperature changes derived from benthic foraminifera isotopic records. Quat. Sci. Rev. 21, 295–305. https://doi.org/10.1016/S0277-3791(01)00101-9.
Wall, D., Dale, B., 1966. "Living fossils" in western atlantic plankton. Nature 211, 1025–1026. https://doi.org/10.1038/2111025a0.
Wold, C.N., 1994. Cenozoic sediment accumulation on drifts in the northern North Atlantic. Paleoceanography 9, 917–941. https://doi.org/10.1029/94PA01438.
Xiao, X., Fahl, K., Müller, J., Stein, R., 2015. Sea-ice distribution in the modern Arctic Ocean: biomarker records from trans-Arctic Ocean surface sediments.

Geochem. Cosmochim. Acta 155, 16–29. https://doi.org/10.1016/j.gca.2015.01.029.
Yeager, S., 2015. Topographic coupling of the atlantic overturning and gyre circulations. J. Phys. Oceanogr. 45, 1258–1284. https://doi.org/10.1175/JPO-D-14-0100.1.
You, D., Stein, R., Fahl, K., Williams, M.C., Schmidt, D.N., McCave, I.N., Barker, S., Niu, L., Kuhn, G., Niessen, F., 2023. Last deglacial abrupt climate changes caused by meltwater pulses in the Labrador Sea. Communications Earth & Environments 4. https://doi.org/10.1038/s43247-023-00743-3.
Zhuravleva, A., Bauch, H.A., Van Nieuwenhove, N., 2017. Last Interglacial (MIS5e) hydrographic shifts linked to meltwater discharges from the East Greenland margin. Quat. Sci. Rev. 164, 95–109. https://doi.org/10.1016/j.quascirev.2017.03.026.